NIS-IPP LA-SUB--96-17

Agreement No. 4528 N 0004-35

between

A. A. Bochvar All-Russian Institute of Inorganic Materials

and

Los Alamos National Laboratory

Report for 1995

Process Optimization for Advanced High Conductivity - High Strength Materials

Development of Cu-Nb Alloy Microcomposite Conductors for High Field Pulsed Magnets

V.I. Pantsyrnyi, A.K. Shikov, A.D. Nikulin, N.M. Belyiakov, I.I.Potapenko, A.E. Vorob'ova, A.G. Silaev, N.I. Kozlenkova, V.G. Zinov'ev, V.A. Drobyshev
Bochvar All-Russia Institute of Inorganic Materials, 123060, Rogov Str. 5, Moscow, Russia

ABSTRACT

The primary goal of this research project is to develop high strength-high conductivity composite wires with enhanced cross-section. For this purpose the following areas of systematic research have been started: melting, deformation, TEM and SEM microscopy, mechanical and electrical characterization of "in situ" Cu-Nb microcomposites. The process of consumable arc melting with the use of initial composite electrodes produced by cold deformation was chosen for preparing initial ingots of Cu-(16-18) wt%Nb alloy. The deformation process including operations of extrusion, drawing with intermediate heat treatments and rolling has been analyzed. The structure of Cu-Nb composite was investigated at all stages of its fabrication. The method of rebundling was successfully used for manufacture of conductors with enhanced cross sections. Wire with 3 x 7 mm^2 cross section and the length of 50m was produced with UTS (20° C) = 1000 MPa and electroconductivity 70% IACS.

I. INTRODUCTION

The main development activity in pulsed magnetic fields is directed towards the ultimate achievement of 100 T in a non-destructive way. It is well understood that the magnet designed for 100 T should be sectioned, which requires the use of quite different materials in different sections. For the inner section of the magnet the further development of high strength, high conductivity conductors, in particular, based on microcomposites of Cu-Nb and Cu-Ag should be done. A lot of investigations have alrady been carried out on Cu-Nb microcomposites for the past 20 years [1-3]. It is well known that the strength of the deformed microcomposites is much greater than calculated from the rule of mixture (ROM). Two groups of models have been proposed to explain this phenomena. The phase barrier model suggested by Spitzig et al [4] and dislocation model proposed by Funkenbush and Courtney [5] both are able to obtain a satisfactorily good description of the strength when proper fitting parameters are used. Very recently Hangen and Raabe [6] proposed an analytical model for the calculation of the yield strength of Cu-Nb microcomposites which is based on the formation of dislocations pile-ups in the Cu matrix and dislocation movement in the Nb filaments. This model regards the yield strength of the composite as the sum of the volumetric

Hall-Patch type contribution attributed to the influence of the Cu-Nb boundaries. The prediction of the model are in the best accordance with experimental data. It is also important to underline that the model is valid only for a well aligned and homogeneous morphology of Nb inclusions, i.e. for $\ln A_0/A > 4$ and uniaxial strain. It should be noted that the Nb deformation are not equal to the calculated deformation of wire as a whole. Heringhaus, Raabe, Gottstein [7] explained this phenomena by at least two reasons. First, the strain distribution during wire drawing is inhomogeneous across the wire diameter, which results in an inhomogeneous dendrite morphology. Second, for $n < 6$ small degrees of deformation cause the initially randomly oriented dendrites to rotate towards an orientation parallel to the wire axis. Only after this alignment a massive cross-sectional area reduction of the dendrites was observed. That is why neither the actual Cu deformation nor the actual Nb deformation equals the true wire deformation.

The objectives of our investigations was therefore to investigate the relationships of microstructure parameters with the mechanical parameters of wire and to optimize the process of Cu-Nb high strength conductors manufacture.

II. RESULTS AND DISCUSSIONS

2.1 General considerations on the strength of Cu-Nb microcomposites.

Due to the minimal mutual solubility of Cu and Nb in solid state, the Cu-Nb alloy microstructure consists of nearly pure Nb inclusions imbedded in practically pure Cu matrix. The phase diagram of Cu - Nb is presented in Fig.1 [8].

The strength of Cu-Nb microcomposite is depending on the following factors:

- volume fraction of Nb;
- dimensions of Nb inclusions in the ingot;
- homogeneity of Nb inclusions distribution in the ingot;
- final dimensions of Nb ribbons in the conductor.

For attaining the maximum values of conductor strength it is necessary to have the volume fraction of Nb in the range of 14 - 20%. It was shown that for the lesser content of Nb (for example 10%) the maximum attained UTS was approximately two times smaller than for the composite with 18% of Nb [9].

The increase of Nb volume fraction larger than 20% leads to the drastic drop of Cu-Nb material's workability.

Dimensions of Nb inclusions and homogeneity of their distribution in the initial ingot is strongly dependent on the method of melting and the technological parameters of chosen melting process.

Final dimensions of Nb ribbons in the conductor are depending on the initial ingot size, technological route of conductor fabrication and the design of conductor itself.

DISCLAIMER

2.2. Melting of initial ingots.

Due to rather high temperature of alloy melting it is clear that to avoid the oxydation of Nb one should use only vacuum melting processes. When choosing the particular method of vacuum melting the following consideration should be taken into account.

The most simple method of induction melting in graphite crucible usually applied for casting of copper based alloys is not favorable for Cu-Nb alloy in first rate because of intensive NbC formation. In spite of reported positive results on deformation of Cu-Nb alloy's ingot with high content of carbon it seems not to be enough relyable process because of the difficulty to control the content of NbC during the melting process.

The most promising method of melting is obviously the consumable arc melting technique.

The principal scheme of arc melting furnace which was used in this work is presented in fig.2. This furnace enables to obtain the ingots with the diameter up to 150 mm and length up to 800 mm.

In this work we used two types of electrodes for arc melting. In first case the electrodes were fabricated by cold drawing the composite billet which contained three Nb rods and four Cu rods in the Cu tube. The dimentions of the billet components were chosen to obtain the ingot with 18 weight % of Nb. The cross section of such electrode at the intermediate stage of deformation process is shown in fig.3.

In the second case the initial electrodes were produced by pouring the Cu melt into the space between six Nb rods in a vacuum induction furnace. Obtained billets were deformed to the final dimension by following extrusion and drawing. The cross section of this type of electrode at the intermediate stage of deformation is presented in fig.4.

In both cases hexagonal rods with key size 4.8 mm were obtained, then they were cut on lengthes 1000 mm and assembled together for fabricating the initial electrodes for the first arc melting.

The high purity electron beam melted copper (99.99%) with RRR not less than 200 and electron beam melted niobium were used for preparing the initial electrodes in both cases.

In spite of the possibility to fabricate the ingots with the diameter up to 150 mm it was experimentally confirmed that the increase of ingot's diameter was accompanied by the increase of nonuniformity in Nb inclusions sizes and their distribution. It is connected with the increase of difference in cooling rates of the melt in peripherical and central areas of ingot, which leads to appropriate difference in structure.

That is why the ingots of 100 mm in dia were produced for following processing. The ingot of 75 mm in dia was produced for processing a monocore

The ingots were machined to a diameter of 98 mm and were deformed by extrusion and drawing down to intermediate size of approximately 10 mm in dia, then cut to measured lengthes and remelted once more in the same furnace for enhancement the homogeneity of microstructure. Due to dendritic morphology of Nb inclusions it is rather difficult to define the average dimensions of the particles with acceptable accuracy. The typical microstructure of ingot is shown in fig.5.

The average size of Niobium particles in initial ingot could be estimated as 10 x10 mm. But it should be noted that even for 100 mm in dia ingots there is still a lot of place for optimization the melting process directed on the elimination of the nonuniformity in Nb particles sizes all over the ingot's body.

2.3 Deformation process

Due to rather large diameter of the ingot the extrusion is the most acceptable following step of the manufacture process. It should be taken into account that because of great difference in mechanical properties of Cu and Nb, which is even more pronounced at higher temperatures, the character of deformation of Nb and Cu is quite different. In fact one could not expect the equality of cross-sectional area reduction of Nb particles and the Cu matrix material during the extrusion. Flukiger et al. [10] investigated the deformation of Cu-Nb powder composed billet by means of extrusion. It was stated that extrusion at 500 ^{0}C in some extent could be accounted as cold extrusion rather than hot one. But our experiments showed that the extrusion at 500 ^{0}C still leads to rearranging of Nb particles in Cu matrix in greater extent than to their deformation [9]. We obtained the approximately equiaxed Nb particles with the average dimensions 8x8 mm after the extrusion. That is why the true strain of Nb was equal to only 0.8 for true strain of extruded rod - 2.4. The typical sructures of extruded rod's cross section are presented at fig.6.

Even the following deformation of wire by cold drawing does not provide the equality of true strains of Nb and the wire. The longitudinal cross section of wire deformed down to 10 mm (see fig.7a) reveals the essential nonuniformity of Nb particle dimensions and the spacings between them.

Only the deformation down to approximately 3 mm which is close to the final dimension for beginning the process of forming the rectangular conductor 3x2 mm^2 eliminates the nonuniformity in Nb filament sizes (fig.7b). But nevertheless in all papers concerned with the in situ microcomposites, strength of wires traditionally is given in dependance of the strain of wire as a whole.

We have investigated the influence of intermediate heat treatments (HT) on the strengthening of Cu-Nb alloy in Cu cladding during the cold deformation. The volume fraction of outer copper was 23%. Cross section of model wire is shown in fig.8.

THE PROCESSING SCHEDULES ARE GIVEN AS FOLLOW:

INGOT, D=75 mm --> EXTRUSION IN Cu CAN --> ROD, D=30 mm -->

--> DRAWING (CD) --> ROD, D=10 mm --> CUTTING IN 4 LENGTHS -->

--> DRAWING WITH INTERMEDIATE HEAT TREATMENTS (HT)
{4 SETS}:

SET A

H.T. H.T. H.T.
800 C,1h. --> 400 C,1h --> 800 C,1h ----------> D=0.3 mm
D=10 mm D=7 mm D=3 mm

H.T. H.T.
--> 400 C,1h --> 700 C,1h ----------> D=0.3 mm
D=7 mm D=3 mm

H.T. H.T.
--> 400 C,1h --> 600 C,1h ----------> D=0.3 mm
D=7 mm D=3 mm

H.T. H.T.
--> 400 C,1h --> 500 C,1h ----------> D=0.3 mm
D=7 mm D=3 mm

H.T.
--> 400 C,1h ----------> D=0.3 mm
D=7 mm

SET B

H.T. H.T. H.T.
700 C,1h. --> 350 C,1h --> 700 C,1h ----------> D=0.3 mm
D=10 mm D=7 mm D=3 mm

H.T. H.T.
--> 350 C,1h --> 600 C,1h ----------> D=0.3 mm
D=7 mm D=3 mm

H.T. H.T.
--> 350 C,1h --> 500 C,1h ----------> D=0.3 mm
D=7 mm D=3 mm

H.T.
--> 350 C,1h ----------> D=0.3 mm

SET C

H.T. H.T. H.T. H.T.
600 C,1h. --> 300 C,1h --> 600 C,1h --> 600 C.1h.--> D=0.3 mm
D=10 mm D=7 mm D=3 mm D = 1 mm

H.T. H.T.
--> 300 C,1h --> 600 C,1h ----------> D=0.3 mm
D=7 mm D=3 mm

H.T. H.T. H.T.
--> 300 C,1h --> 500 C,1h --> 500 C.1h.--> D=0.3 mm
D=7 mm D=3 mm D = 1 mm

H.T.
--> 300 C,1h ----------> D=0.3 mm
D=7 mm

SET D

H.T. H.T. H.T. H.T.
500 C,1h. --> 250 C,1h --> 500 C,1h --> 500 C.1h.--> D=0.3 mm
D = 10 mm D=7 mm D=3 mm D = 1 mm

H.T. H.T. H.T.
--> 250 C,1h --> 400 C,1h --> 400 C,1h.--> D=0.3 mm
D=7 mm D=3 mm D = 1 mm

H.T. H.T.
--> 250 C,1h --> 400 C,1h ----------> D=0.3 mm
D=7 mm D=3 mm

H.T.
--> 250 C,1h ----------> D=0.3 mm
D=7 mm

The mechanical properties of Cu-Nb core in the model wire with different thermomechanical hystories are presented in fig.9. Due to the presence in monocored wire (fig.8) of outer Cu layer the volume fraction of which is 23% the measured data for the samples having the diameter less than 3 mm were recalculated in accordance with ROM. It was assumed that for deformed Cu the value of UTS = 400 MPa and for heat treated - 200 MPa.

It was shown, that heat treatment at the temperature as high as 800 °C

not less then 10 mm (strain of the wire). The rate of the strength increase after the heat treatment was higher than for the wire deformed without heat treatment.

It was also shown that heat treatments of the 3 mm in dia wire at the temperature higher than 600 ^{0}C lead to diminishing of the final wire strength. It is obviously connected with the process of Nb fibres coagulation.

The TEM investigation of microstructure of the samples with different thermomechanical hystories are now in progress.

The analysis of the evolution of Nb filaments form during the deformation process showed that the relationship between actual Nb deformation and actual wire deformation could be divided into three regions (fig.10).

In the first region expedient to the extrusion process, the slope of the line corresponding to the relation between rod deformation and Nb component deformation is very gentle. At this stage the main process is the breaking of dendrites branches and their rearranging almost without changing the Nb particles sizes. In the second region expedient to the beginning of cold drawing, the process of Nb particles reorientation is dominating, but the deformation of some fraction of favourably oriented Nb particles takes place which results in more steep slope of linear dependance. And only in third region, where almost all Nb particles are properly aligned in a composite, the rate of actual strain of Nb increase is close to the rate of actual strain of wire increase.

In accordance with described nature of changing the structure of composite Cu-Nb wire, it is clear that to obtain the necessary structure, which enable to attain the high value of wire strength, one need to deform the wire down to at least 0.3 mm. But it is not possible to use such a wire as a winding material for pulsed magnets, due to quite understandable reasons (low values of filling factor and absolute electroconductivity).

2.4 Rebundling method

We suppose that one of the most acceptable method to attain the necessary high strain of Nb in the wire with cross-section of 6-20 mm^2 is to use the method of rebundling in situ rods in secondary billet with following deformation. The sequence of main steps of rebundling method is presented in fig.11.

We have a great deal of experience in exploring of this method for the production of multifilamentary superconductors. This method seems to be very perspective because of its flexibility for design of various types of high strength Cu-Nb conductors which conductivity and strength are to be optimized for application in outer or inner sections of pulsed magnets. The method of rebundling enables to introduce the needed additional amount of high purity copper inside the conductors by inserting it in the billet in form of rods or sheets.

Several designs of the conductors, produced by the method of rebundling are shown in fig.12.

Geometrical parameters of intermediate Cu-Nb rods to be assembled in the composite billet are defined by the requirement to attain the necessary morphology of Nb filaments in the final conductor. As it was already stated, the diameter of Cu-Nb element in final conductor should be approximately 0.3 mm, which means that the thickness of Nb tapes is equal to 0.1 μm with the spacing between them 0.3 μm. In fig.12 it is shown that the copper may be arranged inside the conductor in different ways - it could be concentrated in the center of the conductor or be uniformly spreaded over the cross-section. We came to conclusion, that the best combinaton of electrical and mechanical properties in one raw with the best conditions of heat exchange between all components of the conductor could be attained when additional copper is uniformly spreaded. Besides abovementioned, this design is preferencial for minimizing the heat generation in bulk copper due to the influence of magnetic field during the pulse. It should be noted that for proper choosing of the thickness of copper layers one should take into account the following consideration. For minimizing the resistivity at a given temperature, it is necessary to minimize the impurity content in copper and to keep the thickness of the copper channels larger than the mean free path of the electrons. Because of pulse magnets usual working temperature equals 77 K the thickness of copper channels should not be less than 10 μm in final conductor.

The strength of such kind of conductor could be calculated in accordance with ROM, assuming the Cu-Nb inserts to be monolithic material with the strength as high as 2,000 MPa. Taking the volume fraction of Cu-Nb component equal to 65% the attainable calculated UTS of the conductor is 1,400 Mpa. The calculated conductivity of this conductor is 70%. Now the work on fabrication of the optimized conductor is in progress.

Meantime, not waiting for the fulfillment of the work on the design optimization, we investigated the influence of heat treatment on mechanical properties and electroconductivity of the 2x3 mm^2 final conductor with copper channels (type 20; fig 10.c). The strength/ conductivity properties measured for this conductor after the various heat treatment regimes are summarized in Table 2 and presented in fig. 13 - 16.

TABLE 2.
SUMMARY OF TENSILE STRENGTHS AND ELECTRICAL CONDUCTIVITIES OF TYPE 20 2x3 mm^2 CONDUCTOR AFTER VARIOUS HEAT TREATMENT REGIMES.

Treatment Regime	Ultimate Tensile Strength, MPa	Yield Strength, MPa	Elong. %	Electr. Conduct. %IACS	RRR77
Initial	990	620	1.9	72	5.37
state	990	610	1.9	72	5.62
200 C,1h vacuum	900	560	1.1	72	6.00
200 C,3h vacuum	890	610	0.8	70	6.27
300 C,1h vacuum	880	620	1.4	70	6.10
300 C,3h vacuum	880	580	1.0	71	6.22
400 C,1h vacuum	860	570	1.1		
400 C,3h vacuum	830	580	2.0	70	6.30
500 C,1h vacuum	720	490	3.8	76	6.20
600 C,1h vacuum	560	400	13.5	80	6.25
700 C,1h vacuum	470	310	16.5	79	6.35
200 C,1h in air	880	550	0.8	74	5.92
300 C,1h in air	880	660	1.8	74	6.12
400 C,1h in air	760	515	1.0	72	6.08
500 C,1h in air	650	460	7.2	73	6.12
600 C,1h forvacuum	525	389	16.0	77	6.30
700 C,0.3h forvacuum	470	310	20.5	82	6.50

2.5 Electroconductivity

2.5.1. General considerations on the conductivity of Cu-Nb microcomposites.

It is well known that conductivity of strongly deformed microcomposites are determined by their microstructure [11]. All principal mechanisms of strengthening of Cu-Nb microcomposites - the formation of the filamentary structure with the characteristic interfilament spacing 0.1-1 μm, the creation of high dislocations density - provide the decrease in microcomposite electroconductivity. The only traditional way of increasing strength by providing finely dispersed precipitates may cause a certain increase in conductivity due to the refinement of the copper matrix. Such situation was described by Sakai [12] for the Cu-Ag system.

Taking into account anticorrelation between conductivity and strength, it would be important to find out which of the scattering mechanisms in microcomposites gives the maximum contribution into electrical resistivity.

The main factors, which determine the scattering of electrons in microcomposite are as follow:

- Nb fibres surfaces (size effect);
- impurities;
- dislocations;
- mutual solubility of microcomposite's components;
- fine dispersive inclusions of Nb in copper matrix.

The mechanisms of electron scattering in same way as the mechanism of strengthening in "in situ" microcomposites are different at the different stages of fabrication and are determined by the characteristics of microstructure.

Increase of deformation degree leads to the microcomposite microstructural changes, density and dislocation structure which in turn leads to the appropriate changes in physical properties of microcomposite itself.

We have begun carrying out the straight measurements of dislocations density. It is very difficult to define the dislocation density by TEM due to the fact that at high values of dislocations density the dislocation images are of the same order as the distances between the dislocations. That is why for comparison we also use the method of determination of the dislocations density by calculating it out of X-ray measurements. This work is now well in progress. The preliminary results have shown that the dislocations density in the Nb filaments for the final conductor defined by TEM analysis is almost in an order of magnitude lesser than obtained out of X-ray measurements and equels to 8×10^{10} cm^2 and 3×10^{12} cm^2 appropriately.

In accordance with the experimental data obtained by Bevk [13] for Cu-Nb microcomposites cold deformed up to $\ln \mu = 8$ the concentration of dislocations in Nb filaments were estimated as 10^{13} cm^{-2}, which were more than the order of magnitude higher than the usual values for cold deformed monomaterials. But it should be also noted that in the Nb filaments with the thickness of 10 - 20 nm the dislocations were not found at all. Increase of dislocation density up to 10^{12} - 10^{14} cm^{-2} at the degree of cold working $\ln \mu = 5$

50-10 nm for Cu-Ag system have been also stated by Frommeyer in [14]. Absence of dislocations in very fine filaments with the diameters of 10 nm have been explained by the impossibility of dislocations generation in accordance with Frank-Reed mechanism. The high level of dislocations density was also mentioned by Embury [15] on the base of the experiments on etching out the Nb filaments. The strong curling of filaments witnessed about high level of residual stresses in the composite. Embury [15] made a conclusion that due to very high dislocation density the process of their annigalation is probable even at low temperatures.

Being pinned to interfacial surfaces dislocations could not be very effective centres of electrones scattering, that is why the dislocation mechanism of electron scattering could not be accounted as a main one for strongly deformed microcomposites.

Let us estimate the input of dislocation density to the decrease of electroconductivity taking into account abovementioned considerations. It is known that the increase of resistivity on the single dislocation is varied from 10^{-21} up to 10^{-20} Ohm$\otimes$cm, depending from orientations of dislocation and current [16]. Higher estimations of the resistivity increase 10^{-19} Ohm$\otimes$cm made in [17] obviosly was connected with the input of point defects associated with dislocations. For plastically deformed copper the increase of resistivity associated with dislocations was estimated as approximately 2% [16].

Summarizing all abovementioned one could expect the increase of resistivity connected with high dislocations density in the range of 0.1 - 1 μOhm x cm for the microcomposites.

The scattering of electrons on interfacial surfaces at the first time have been investigated by Fuks, Sondheimer and Dingle [17] for thin films. Electroconductivity in the thin film with thickness $t < \lambda_b$ can be expressed by following expression:

$$\sigma/\sigma_b \sim 3/4 \cdot (t / \lambda_b) \cdot \ln(\lambda_b / t)$$

where σ, σ_b - conductivities of film and bulk samples accordingly;

λ_b - mean free path of electron in bulk specimens.

The use of this expression for microcomposites gives a satisfactorily good agreement with experiment [18].

The influence of size effect on the electroconductivity of heavily deformed "in situ" microcomposites is strong for the case when the mean free path of electron (λ_b) in all components is lesser than the length of the filaments (D) and more than interfilament distance (δ).

In case when $\lambda_b > D$ the local decrease of electroconductivity in the interfilament material does not influence on the electroconductivity as a whole [19].

The size effect seems to be the main factor which define the microcomposites electroconductivity.

Impurities in microcomposites are influencing on the conductivity and

copper and Nb for fabrication of the conductors and pay attention for chosing the proper way of melting not to introduce possible additional impurities during the melting process.

Precipitations of second phases in copper matrix could lead to slight increase of electroconductivity due to the purification of copper. But if such precipitates create the lattice with period coincidental with mean free pass of electron, these precipitates would be themselves the centres of electron scattering.

2.5.2 Experimental part

Electrical resistivity was determined by the DC four-probe technique. The voltage was measured with the sensibility not worse than $5x10^{-8}$ V. The error in determination of the electroconductivity was determined mainly by the error in determination of the geometrical dimensions of the sample and was estimated to be 4%. The accuracy of RRR 77 measurements was equal to 0.5 %.

Experimental probes enabled the measurements in the temperature range from 300 K to 4.2 K. The probe consisted of sample holder and heating chamber with the thermometer. The sample was mounted very close to cryogenic charcoal thermometer. Sample holder with the sample was mounted in evacuated can, filled with gaseuos helium at room temperature.

2.5.3 Results and discussion

As it was mentioned above we used copper with resistivities ratio RRR 4.2 = 400 and 140. The RRR values of specimens upon melting, drawing and heat treatment at 500 ^{0}C for 1 h were estimated to be 145 and 28, respectively. The conductivities of remelted copper were used in the calculations of the conductivity of composites.

Some experiments have been carried out on melting the copper in graphite and yttria ceramic crucibles. It was shown that RRR parameter of copper casted into yttria crucible was almost two times higher than the RRR of copper casted in graphite crucible. Consequently, melting in graphite crucible could be accompanied by saturation of copper with gaseous impurities in first rate with sulfur from graphite crucible, which considerably reduces the conductivity of copper. According to Verhoeven et al. [20], impurities entering copper while melting also determine, to a large extent, mechanical properties of the composites. For this reason, initial Cu and Nb must be purified and melting must be conducted in the atmosphere free of oxygen, in crucibles not evolving sulfur. Merely such conditions allow deformation of Nb to a small diameter. That is why we developed the process of fabrication the initial composite Cu-Nb electrode only on the base of mechanical reduction without including induction melting.

As it was stated in chapter 5.2.1 the electroconductivity of microcomposites is strongly influenced by microstructure. The degree of deformation and structural characteristics of some of investigated samples are given in the table 3 for the Cu -16 wt.% Nb specimens obtained from copper with RRR = 140 (specimens 1 - 5) and RRR = 400 (specimen 6)

TABLE 3.
DEFORMATION AND NB INTERFILAMENT SPACINGS IN THE CU 16% NB SPECIMENS (500 °C, 1H).

№	wire diametr, mm	lnμ wire	Nb cross section, μm	interfil. spesing, μm
1	10.0	4.6	2.1x5.2	4.7
2	3.0	6.4	0.7x3.0	2.0
3	0.8	9.4	0.2x1.7	0.7
4	0.6	10.6	0.1x1.2	0.6
5	0.3	11.6	0.1x1.0	0.3
6	2x3	11.8	0.1x1.0	0.4

It should be noted that the size of Nb inclusions and interfilament spacing are greatly dispersed: the distance between Nb particles in the specimen of 10 mm in diameter ranges from 0.3 to 12 μm and from 0.8 to 6 μm in the specimen of 3 mm in diameter. The table contains the mean values of Nb particle size and the interfilament spacing.

With an increase in the degree of deformation, the structure of a Cu-Nb conductor changes from that with separate Nb particles dispersed in the copper matrix to the structure with Nb filaments.

The conductivity of specimens with the filamentary structure is equal to the sum of the component conductivities:

$$\sigma^* = V_1 \cdot \sigma_1 + (1 - V_1) \cdot \sigma_2 \qquad (1)$$

where: V_1, $V_2 = 1 - V_1$, σ_1 and σ_2 are the volume fractions and conductivities of Nb and Cu, respectively.

A number of studies, including the comprehensive review of Hale [21], are devoted to the calculation of in situ composites containing inclusions of the second component. Good agreement with experiment is provided by the Landauer formula [22]:

$$\sigma^* = 1/4\{(3V_2 - 1)\cdot\sigma_{Cu} + (3V_1 - 1)\cdot\sigma_{Nb} + [\{(3V_2 - 1)\cdot\sigma_{Cu} + (3V_1 - 1)\cdot\sigma_{Nb}\}^2 + 8\cdot\sigma_{Nb}\cdot\sigma_{Cu}]\}^{1/2} \qquad (2)$$

Insignificant difference between the calculated and experimental values was noticed for the systems with mutual solubilities of components. In accordance with the phase diagram (see fig.1), the equilibrium solubility of Nb in Cu is 0.2 wt.%. The effect of Nb additions on copper conductivity can be estimated by comparing the results of the calculation with experimental data for the specimens containing isolated Nb particles in the copper matrix.

The microcomposites conductivities at 300 K referred to the conductivity of copper upon melting and subsequent heat treatment, appropriate for a particular conductor, are plotted in Fig. 2. The plots obtained with the use of

The conductivity of specimen 1 at 300 K, 77 K and 4.2 K is well described by formula (2). It means that the structure with continuous filaments is really still not formed at the degree of deformation $\ln \mu < 4.6$. The absence of transition to superconducting state at the temperature of liquid helium for the sample 10 mm in dia also confirmed this statement. It was observed that copper conductivity was not affected markedly by Nb dissolved in Cu.

The conductivity of the specimen of 3 mm in diameter at 300 K is well described by equation (1). Although the structure of specimens of 0.8 mm or less in diameter and conductors of 2 mm x 3 mm cross section admits the use of formula (1) for calculating conductivity, the results obtained at 300 K fall below the $\sigma^*/\sigma_{Cu} = f(V_1)$ curve calculated for the filamentary structure.

The experimental σ^*/σ_{Cu} values obtained at 77 K and 10 K for the specimens of 3 mm or less in diameter fall much lower than the calculated by formulas (1) and (2) values. This data confirm that the conductivity of copper in filamentary composites is significantly lower than the conductivity of copper contained equal volume fraction of equaxed Nb inclusions.

The estimates of the copper conductivity in the composite using formulae (1) and (2) and comparison of the results with Sondheimer's curve [23] showing a decrease in conductivity due to the scattering at the boundaries give qualitative agreement on account of significant errors involved in determining the interfilament spacing and copper conductivity in the composite (Fig. 18).

Good coincidence of calculated and experimental data could be observed in case when interfilament spacings would be in a factor of 2.5 lower than determined out of micrographs.

Thus, the discrepancy between the calculation σ^*/σ_{Cu} by formula (1) and the experimental data observed on the specimens of 3 mm or less in diameter at low temperatures can be attributed to the size effect.

Comparison of the λ_b values at 300 K ($\sim 0.03\mu m$) with the interfilament spacing shows that the size effect for all specimens studied should not affect conductivity. The discrepancy between the calculation and experiment at 300 K for the specimen of 3 mm or less in diameter requires special consideration.

Figure 19 shows the conductivity of MC specimens, measured at 300 K, 77 K and 10 K as well as Cu conductivity (insert in figure) as a function of the temperature of heat treatment.

An increase in copper conductivity caused by the heat treatment and the saturation beginning at a temperature above 250 ^{0}C (insert in Fig. 19) are characteristic of the recristallization process. After additional heat treatment at 700 ^{0}C in air, the conductivity of copper and composite conductor considerably increases, and the RRR parameter reaches the values of 127 and 124 for Cu and 10-mm in situ conductor, respectively. The conductivity of composites increases with the temperature of heat treatment. It could be explained by the increase of interfilament spacing which is the sequence of the process of Nb filaments coagulation. As a result the influence of size effect on conductivity is strongly reduced.

The fig.19 shows that for the sample with Nb filaments 0.1 x 1.0 μm and interfilament spacing 0.4 μm the increase of conductivity take place at temperature lower than it happens for the sample with Nb filaments with cross section of 0.2 x 1.7 μm. Our data are in good agreement with the data of Embury on the temperatures of Nb spheroidization.

Fig.20 also illustrates the effect of deformation on the conductivity of specimens heat treated at 500 ^{0}C for 1 h. The sharp decrease in conductivity at low temperatures is observed for ln $\mu > 4.7$, the point when the structure of the samples becomes to be filamentary.

At fig.21 the relationships between resistivity and degree of deformation for cold deformed and heat treated at 500 ^{0}C samples with filamentary structure are presented. It is shown that characters of the curves were quite different:
- practically linear diminishing of conductivity with the increase of deformation degree for heat treated samples is obviously the sequance of only one mechanism of the conductivity changing dominating for these samples.

The curve corresponding to heavily cold deformed samples goes practically parallel to the curve corresponding to heat treated samples until the value of strain ln $\mu = 9.8$ is attained. The sharp decrease in conductivity is observed for ln $\mu > 9.8$.

This change of curve steepness is connected with corresponding change in microstructure. Now the work on systematic TEM investigations of structure is in progress.

Consider now the correlation between the tensile strength and conductivity measured at 300 K. Fig. 22 shows the results obtained on the specimens of the Cu-(15-18)% Nb composition in A.A. Bochvar institute and those taken from other sources. Arrows indicate the IACS values (in %) for Cu-16% Nb corresponding to the filamentlike structure (the additive law for conductivity) and to the structure with inclusions of Nb particles (Landauer's formula). The linear correlation between σ^* and σ_B is observed for conductors with the filamentary structure (0.8 mm) , as-drawn and heat treated at temperatures up to 600 ^{0}C. It is violated, however, for the specimens annealed at higher temperatures.

Analysis of the whole set of experimental data and, in particular, the comparison of conductivity calculated with the use of equation (1) with the experimental data obtained at 300 ^{0}C suggests that the interfilament spacing in the specimens of 0.8 mm or less in diameter can be 2.4 times lower than that measured on micrographs. The decrease of the effective interfilament spacing that determines the scattering of conduction electrons in the copper regions of the composite could be associated with two obstacles:

- the presence of the layer with high dislocation density and high resistivity in the boundary region of Cu-Nb composite;
- the process of Nb filament coagulation accompanied with appropriate increase of interfilament spacings.

The schematic representation of the microcomposite structure and the equivalent electrical scheme are shown in Fig. 23. The local dislocation

mean concentration of dislocations. The increase in resistivity at $N_D \sim 10^{14}$ cm^{-2} and at higher N_D values may be as high as $\sim 10^{-6}$ Ohm x cm, if $\Delta\rho$ for a single dislocation varies from $1.3 \cdot 10^{-20}$ to $4 \cdot 10^{-21}$ Ohm x cm [17]. Thus, the effective interfilament spacing may be much lower than the spacing derived from the micrographs, and conductivity may be influenced by the size effect even at 300 K.

Heat treatment may cause both annihilation of dislocations at the boundary with Nb and spheroidization of Nb at temperatures above 300 ^{0}C [18]. As a result, the decrease in the thickness of the dislocation saturated layer and increase in conductivity due to the reduction of the size effect may occur. The intense spheroidization of Nb at temperatures above 600 ^{0}C (for the specimens of 0.8 mm in diameter) is accompanied by the sharp decrease in tensile strength.

2.5.4. Conclusion

To summarize, we have studied the dependence of conductivity on the composition of the microcomposites (in the range 14-20 wt.% Nb) and the structure varying in the process of deformation and heat treatment. The increase in conductivity was observed in going from the structure with Nb particles distributed in the copper matrix to the structure with quasicontinuous Nb filaments. With further deformation (at $\ln \mu > 0.4$), the decrease in the interfilament spacing gives rise to an additional electron scattering at the Cu-Nb boundary and, consequently, to the drop in conductivity. The effective interfilament spacing both in as-drawn and heat treated (up to 600 ^{0}C) condition of the specimens is less than that determined from micrographs. It should be noted once more that even after extremly large deformation nonuniformity in dimensions of ribbontype filaments exists what can be easily seen in SEM micrograph of longitudinal section Cu-Nb wire with 0.8 mm in dia (fig.24) We also assume that the regions near the Cu -Nb boundary with high local dislocation density are responsible for the decrease of the effective (for the scattering of conduction electrons) interfilament spacing.

The distinct correlation between strength and conductivity is observed for the specimens with the filamentary structure, as-drawn and heat-treated up to 600 ^{0}C. The linear behavior of the $\sigma^* = f(\sigma_B)$ curve is violated for the specimens heat treated at $T > 600$ ^{0}C, in which intense Nb spheroidization takes place in the Cu-Nb composite.

It was shown that the considerable drop in conductivity of the composite is due to the saturation with impurities (largely, perhaps, with sulfur) in melting.

III. CONCLUSIONS

The relationships of microstructure parameters with the mechanical and electrical parameters of wire have been investigated. It was confirmed that due to the typical for bcc materials <110> texture in the Nb on drawing, the Nb filaments transform in a ribbon-shaped cross-section with the ratio of cross-sectional dimensions reaching a factor of 10.

It was shown that in order to develop an optimized for pulsed magnets high strength, high electroconducting material on the base of Cu-Nb alloy it is necessary to use the rebundling method. Several types of such conductors with different volume fraction of copper and Cu-Nb alloy were fabricated, including the wires with cross sectons 3x4 mm^2 and 3x7 mm^2. The maximum UTS values of 1100 MPa and conductivity of 73-76% IACS were attained for these conductors. The possibility to attain the UTS value up to 1400 MPa for Cu-Nb conductors with enhanced (up to 20 mm^2) cross-sections have been shown.

REFERENCES

[1] J.P.Harbison, J.Bevk. J.Appl.Phys.,1977, vol.48, no.2, p.p.5180-87.

[2] Шиков, И.И. Давыдов, В.И. Панцырный и др. Исследование процессов получения высокопрчных материалов на основе сплава Cu-Nb" в сб. "Высокотемпературная сверхпроводимость" ВИМИ вып. 4, 1989, стр. 34-39.

[3] J.T.Wood "High-strength, High-conductivity, two-phase materials" Ph.D. Thesis, McMaster University, 1994.

[4] W.A.Spitzig. Acta Metall., 1991, vol.39, p.p.1085-88.

[5] P.D.Funkenbush and T.H.Courtney, Scripta Met., 1989, vol.24, p.p.1719-24.

[6] U.Hangen, D.Raabe "Modelling of the yield strength of a heavily wire drawn Cu-20%Nb composite by use of a modified linear rule of mixtures" Acta Metall. in press.

[7] F.Heringhaus, D.Raabe, G.Gottstein "On the correlation of microstructure and electromagnetic properties of heavily cold worked Cu-20%Nb wires" Acta Metall. in press.

[8] Терехов, Л.Н. Александрова "Диаграмма состояния медь-ниобий" Металлы, т.4, стр. 210-213, 1984.

[9] J.Bevk and K.K.Karasek in "New Developments and Applications in Composites", D.Kuhlmann-Wilsdorf and W.C. Harrigan, eds. AIME, Warrendale, PA, 1979.

[10] R.Flukiger, R.Akihama, S.Foner et al. IEEE Trans.on Magn.,1979, vol.MAG-15, no.1.

[11] W.A.Spitzig,A.R.Pelton and F.C.Laabs "Characterization of the strength and microstructure of heavily cold-worked Cu-Nb composites" Acta Metall., v.35, no.10, p.p.2427-2442, 1987.

[12] Y.Sakai. K.Inoue, T.Asano and H.Maeda "Development of a high strength. high conductivity Copper-Silver alloy for pulsed magnets",

[13] J.Bevk, J.P.Harbison, J.L.Bell "Anomaleous increase in strength of in situ formed Cu-Nb multifilamentary composites", J.Appl.Phys.,vol.49, p.p.6031-6039, 1979.
[14] G.Frommeyer, G.Wassermann "Microstructure and anomaleous mechanical properties of in situ-produced silver-copper composite wires", Acta Metallurgica, v.23, p.p.1353-1360, 1975.
[15] J.D.Embury "Micromechanical descriptions of heavily deformed materials", Scripta Metallurgica et materialia, vol.27, p.p.981-986, 1992.
[16] F.J.Blatt "Theory of mobility of electrons in solids", New York, Academic, 1957.
[17] J.M.Ziman "The theory of transport phenomena in solids", Oxford, Clarendon Press, 1960.
[18] I.N.Gubkin, N.I.Kozlenkova, A.D.Nikulin, M.I.Polikarpova, V.Ya.Filkin "Experimental investigation of copper matrix longitudinal resistance in a composite Nb-Ti wire", IEEE Trans. Magn., vol.30, p.p.2372-2374, 1994.
[19] G.Horvath, J.Bankut "Role of size effect in the stabilization of in situ superconducting tapes", Cryogenics, vol.29, p.p.931-934.
[20] J.D.Verhoeven, W.A.Spitzig, L.L.Jones, H.L.Downing et al. "Development of deformation processed copper-refractory metal composite alloys "J.Mater.Eng., vol.12, p.p.127-139, 1990.
[21] D.K.Hale "The physical properties of composite materials" J. Mater. Sci., vol.11, p.p.2105-2141, 1976.
[22] R.Landauer "The electrical resistance of binary metallic mixtures", J. Appl. Phys., vol. 23, p.p.779-784, 1952.
[23] E.Sondheimer, Advan.Phys., vol.1, p.12, 1952.

FIGURE CAPTIONS

Fig.1 Cu - Nb phase diagram

Fig.2 Principal scheme of arc melting furnace.

Fig.3 Cross section of initial composite Cu-Nb electrode fabricated by cold drawing.

Fig.4 Cross section of initial composite Cu-Nb electrode. fabricated by casting.

Fig 5. Microstructure of the Cu-18%Nb ingot.
a) peripherical area of the ingot
b) central area of the ingot

Fig.6. Microstructure of the extruded rod

Fig.7. Microstructure of the Cu-18%Nb rod.
a) 10 mm in dia. b) 3 mm in dia.

Fig.8. Cross section of Cu-18%Nb wire in Cu cladding.

Fig.9a. Room temperature tensile strength (UTS) versus logarithmic strength for model Cu-Nb wire deformed with intermediate heat treatments (Set A)

Fig.9b. Room temperature yield strength (YS) versus logarithmic strength for model Cu-Nb wire deformed with intermediate heat treatments (Set A)

Fig.9c. Room temperature elongation values (El) versuslogarithmic strength for model Cu-Nb wire deformed with intermediate heat treatments (Set A)

Fig.9d. Room temperature tensile strength (UTS) versus logarithmic strength for model Cu-Nb wire deformed with intermediate heat treatments (Set B)

Fig.9e. Room temperature yield strength (YS) versus logarithmic strength for model Cu-Nb wire deformed with intermediate heat treatments (Set B)

Fig.9f. Room temperature elongation values (El) versus logarithmic strength for model Cu-Nb wire deformed with intermediate heat treatments (Set B)

Fig.9g. Room temperature tensile strength (UTS) versus logarithmic strength for model Cu-Nb wire deformed with intermediate heat treatments (Set C)

Fig.9h. Room temperature yield strength (YS) versus logarithmic strength for model Cu-Nb wire deformed with intermediate heat treatments (Set C)

Fig.9i. Room temperature elongation values (El) versus logarithmic strength for model Cu-Nb wire deformed with intermediate heat treatments (Set C)

Fig.9j. Room temperature tensile strength (UTS) versus logarithmic strength for model Cu-Nb wire deformed with intermediate heat treatments (Set D)

Fig.9k. Room temperature yield strength (YS) versus logarithmic strength for model Cu-Nb wire deformed with intermediate heat treatments (Set D)

Fig.9l. Room temperature elongation values (El) versus logarithmic strength for model Cu-Nb wire deformed with intermediate heat treatments (Set D)

Fig.10. Relationship between true strains of Nb filaments and the wire as a whole.
I region - corresponds to extrusion operation
II region - corresponds to the beginning of drawing
III region - corresponds to the extensive drawing

Fig.11. Rebundling method processing procedures

Fig.12. Cross-sections of 2x3 mm2 Cu-Nb conductors
with different amount of pure copper.
a) %Cu 2x3 mm^2
b) %Cu 2x3 mm^2
c) %Cu 2x3 mm^2
d) 2x3 mm^2
e) 2x3 mm^2
f) 3x4 mm^2
g) 3x7 mm^2

Fig.13. Room temperature electroconductivity versus annealing temperature for heat treating in vacuum and in air.

Fig.14. Residual Resistivity Ratio {RRR 77K} versus annealing temperature for heat treating in vacuum and in air.

Fig.15. Room temperature tensile strength (UTS), yield strength (YS), elongation (El) versus annealing temperature for heat treating in vacuum and in air during 1 hour.

Fig.16. Room temperature tensile strength (UTS), yield strength (YS), versus annealing duration for heat treating in vacuum.

Fig.17. Comparison of calculated and experimental values for Cu-Nb microcomposite conductivity.

Fig.18. The resistivity of Cu (ρ_L /ρ_b) in Cu-16%Nb wire as a function of interfilament spacing (δ/λ_b).

Fig.19. Conductivity of Cu-16%Nb as a function of heat treatment temperature.

Fig.20. Conductivity as a function of deformation.

Fig.21. Resistivity as a function of deformation.

Fig.22. Correlation between ultimate tensile strength and conductivity.

Fig.23. Schematic of a structure of microcomposite and its electric equivalent.

Fig.24. Longitudinal section of 0.8 mm in dia Cu-Nb wire.

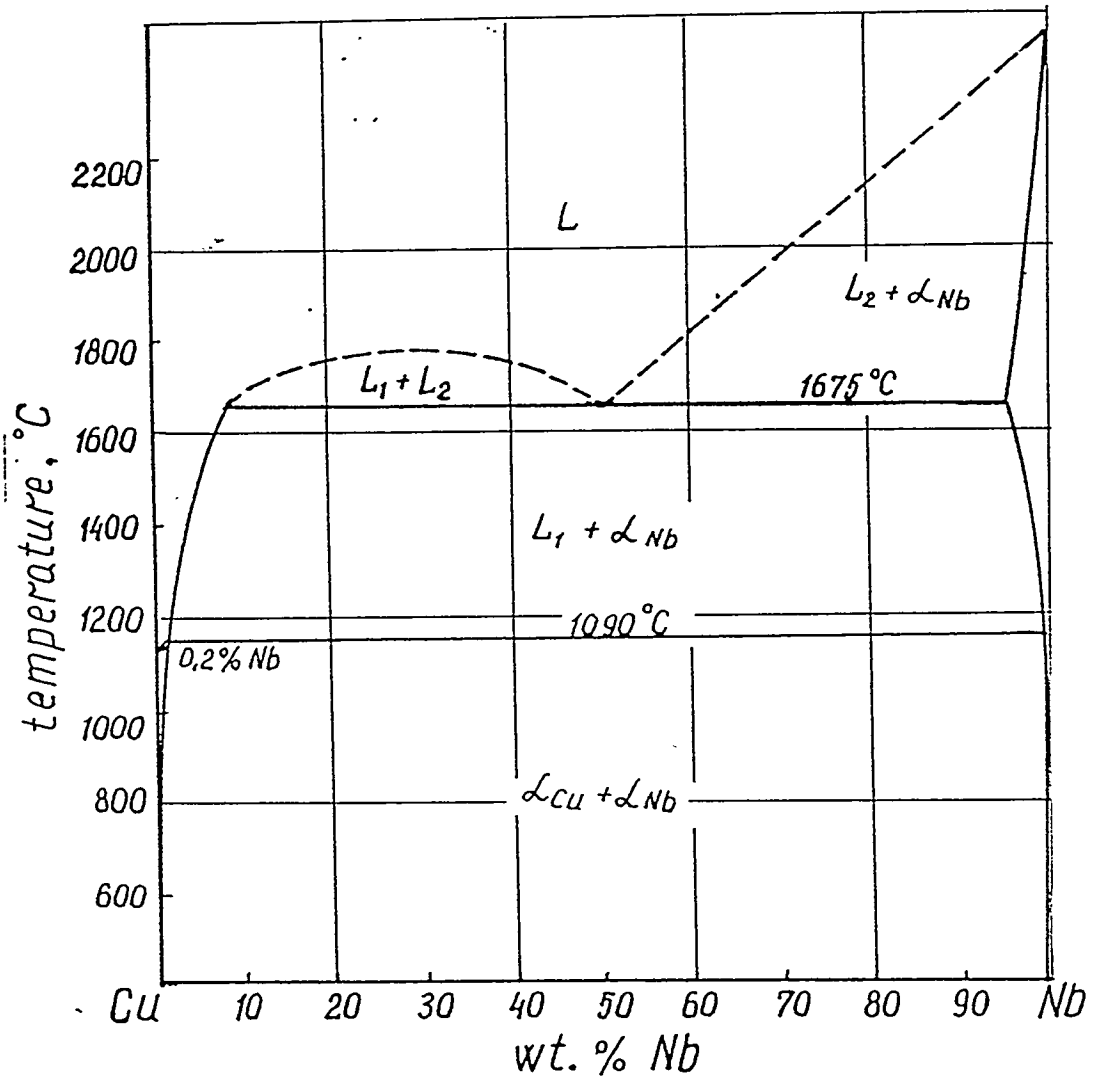
2200
2000
1800
1600
1400
1200
1000
800
600
temperature, °C
L
$L_2 + \alpha_{Nb}$
$L_1 + L_2$
1675 °C
$L_1 + \alpha_{Nb}$
1090 °C
0.2% Nb
$\alpha_{Cu} + \alpha_{Nb}$
Cu
10
20
30
40
50
60
70
80
90
Nb
wt. % Nb

Fig. 1

ARC-MELTING FURNACE

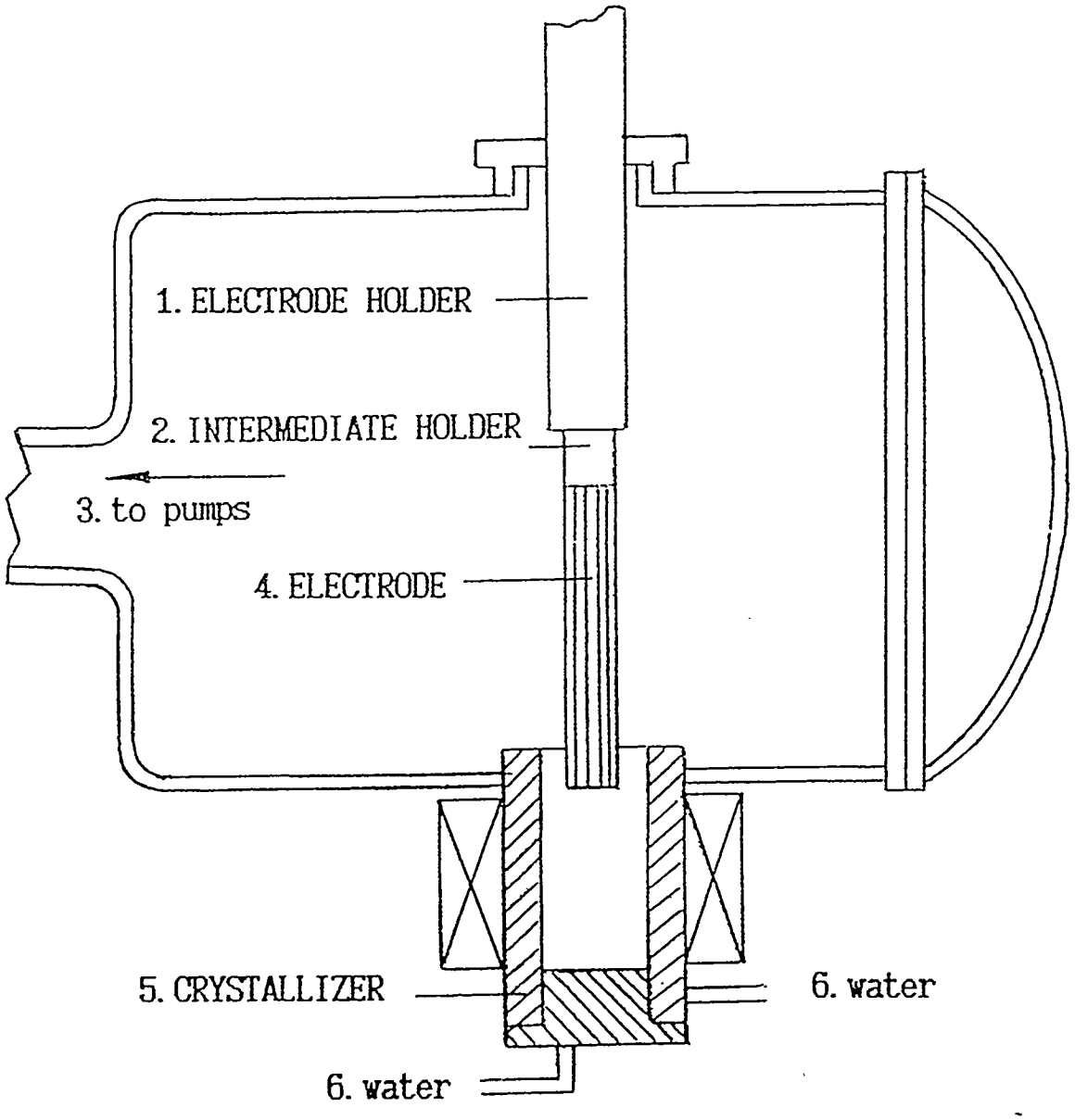

Fig. 2

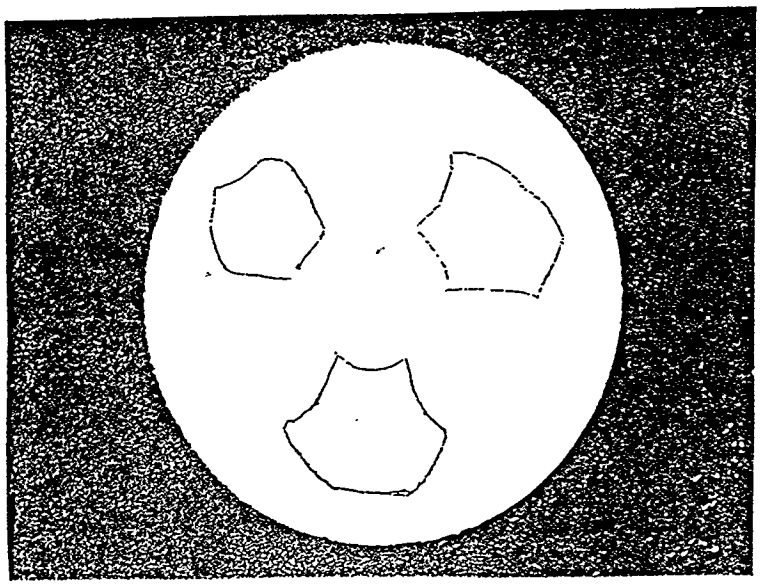

Fig. 2

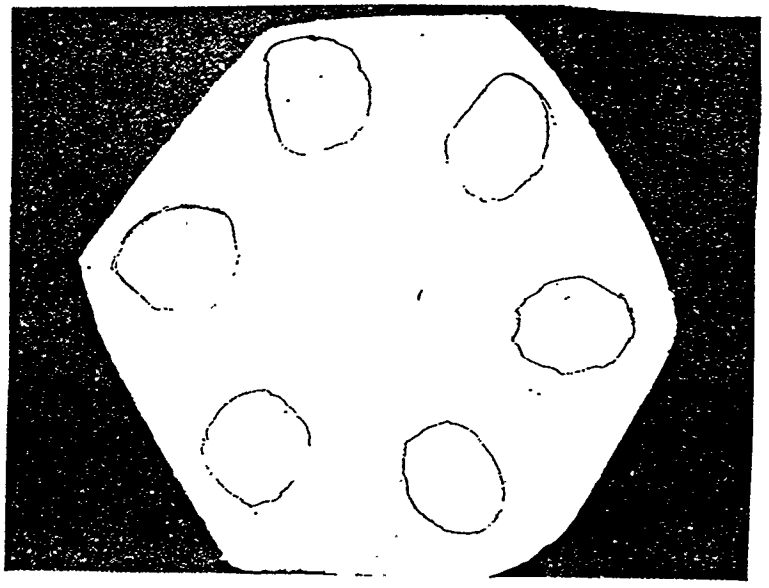

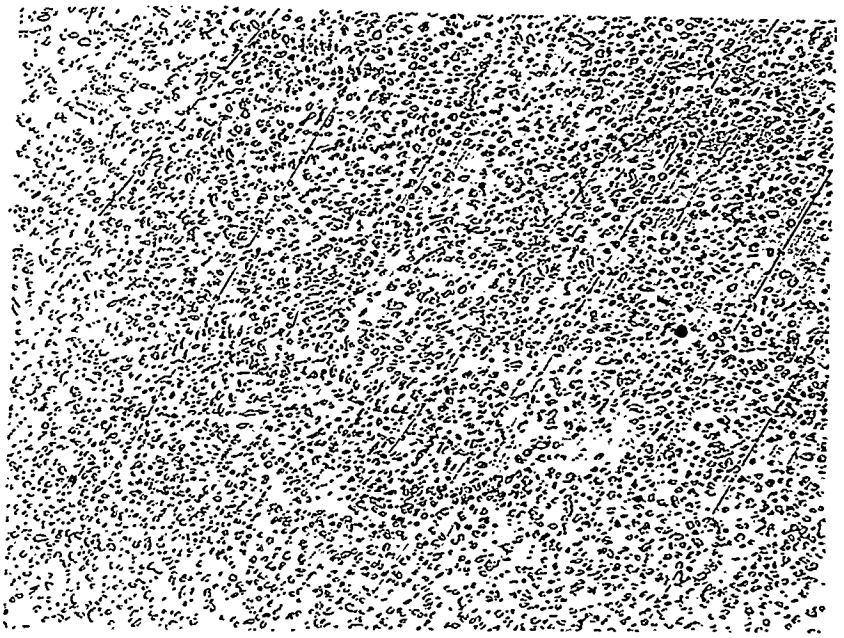

а

в

Fig. 5

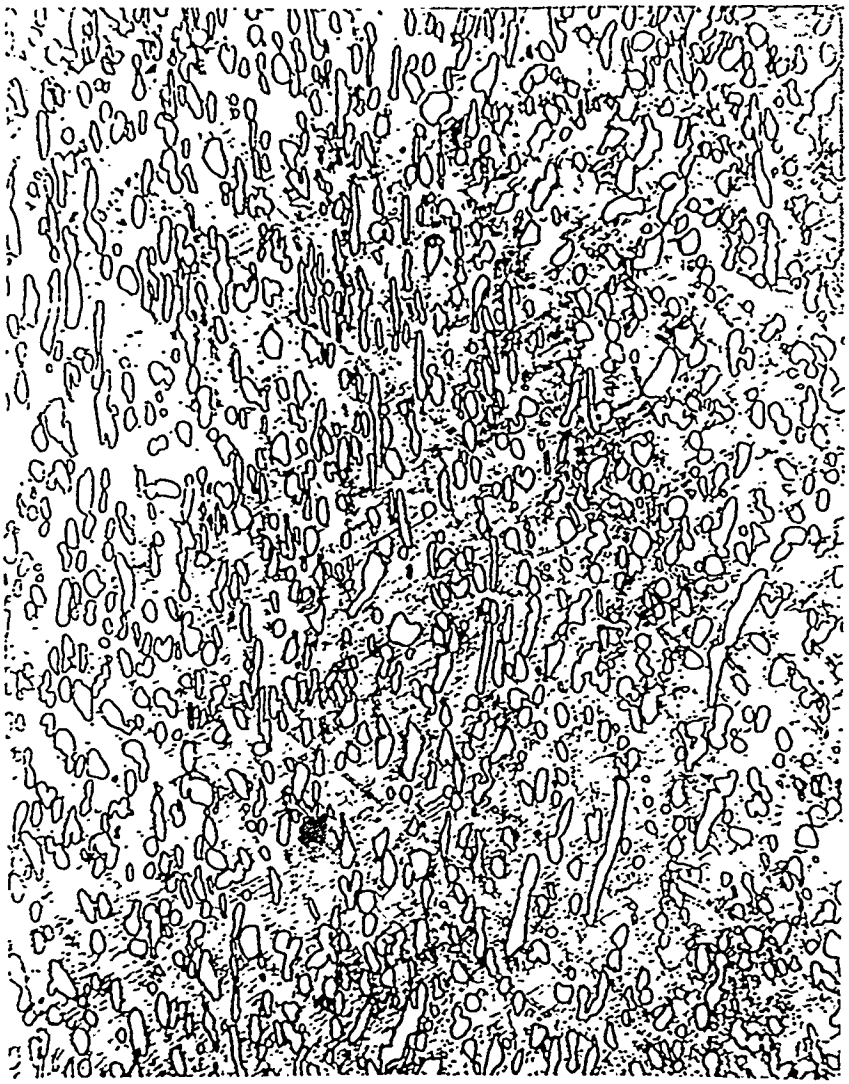

Fig. 6

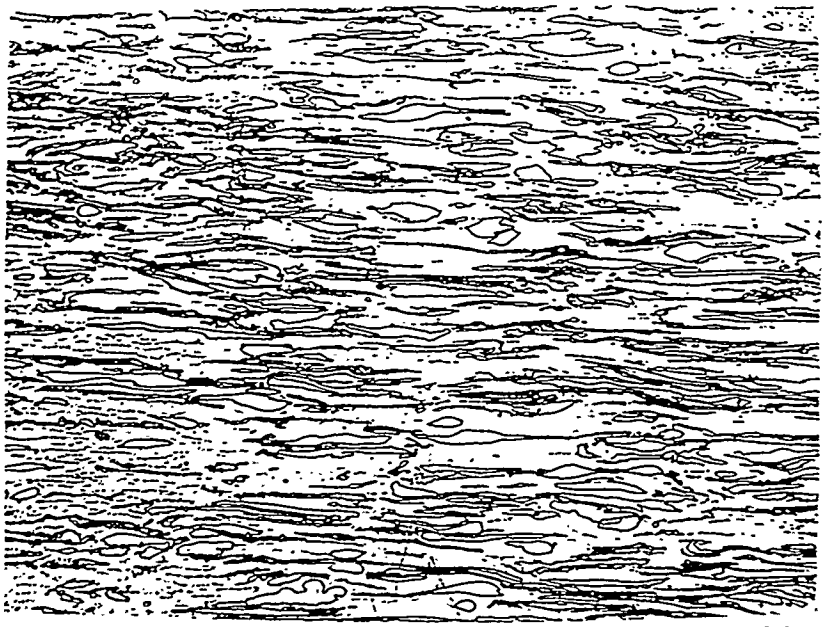

a

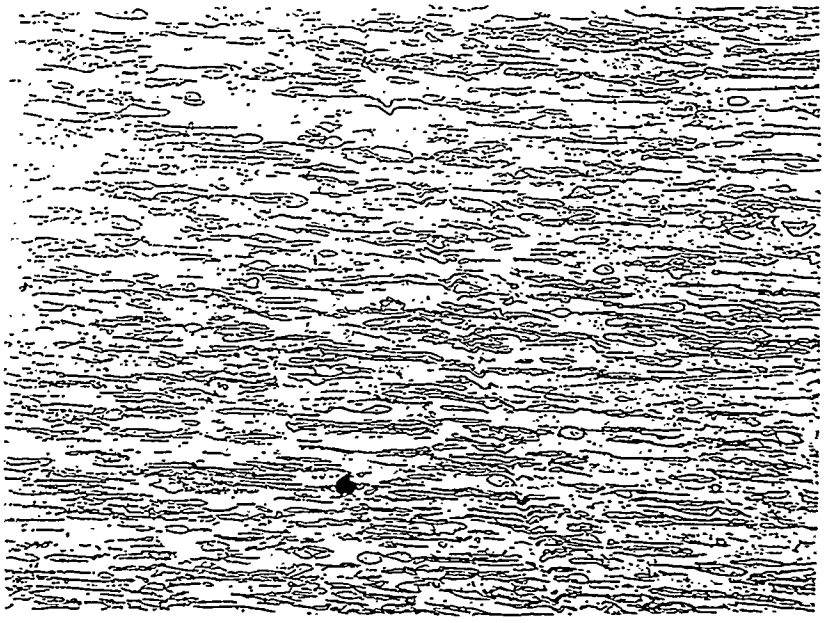

b

Fig. 7

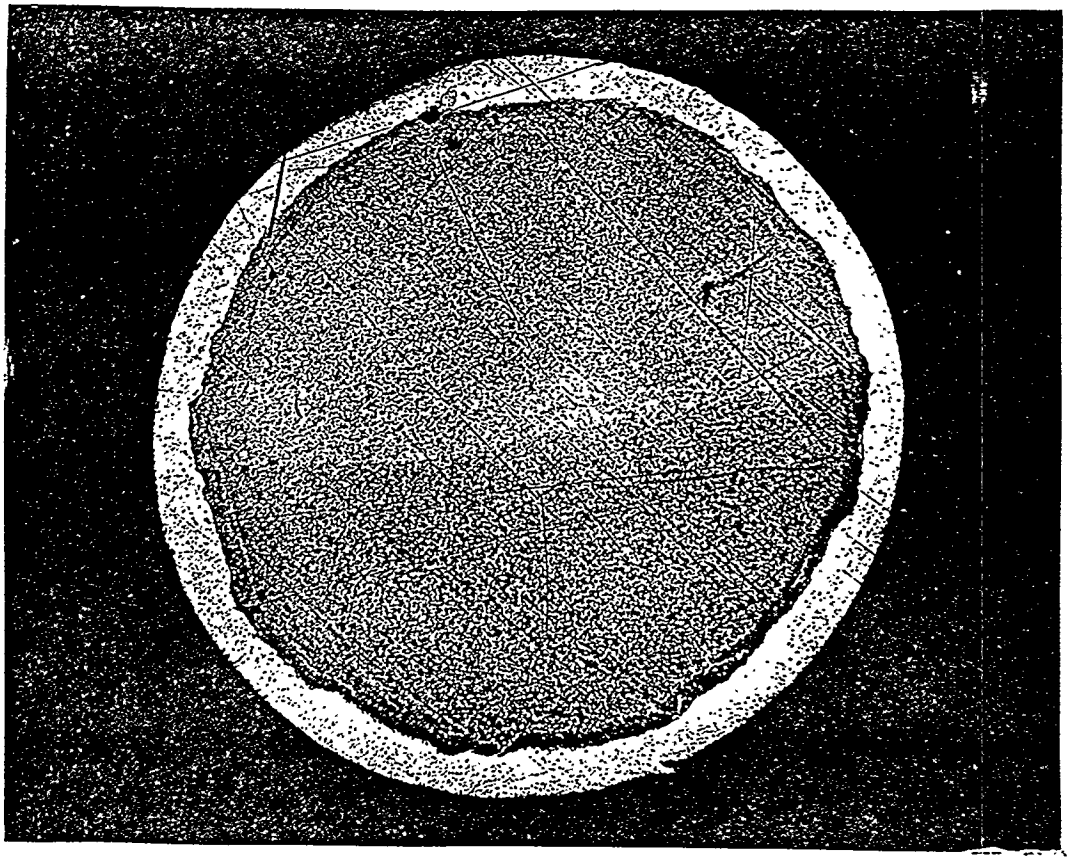

x125

Fig. 8

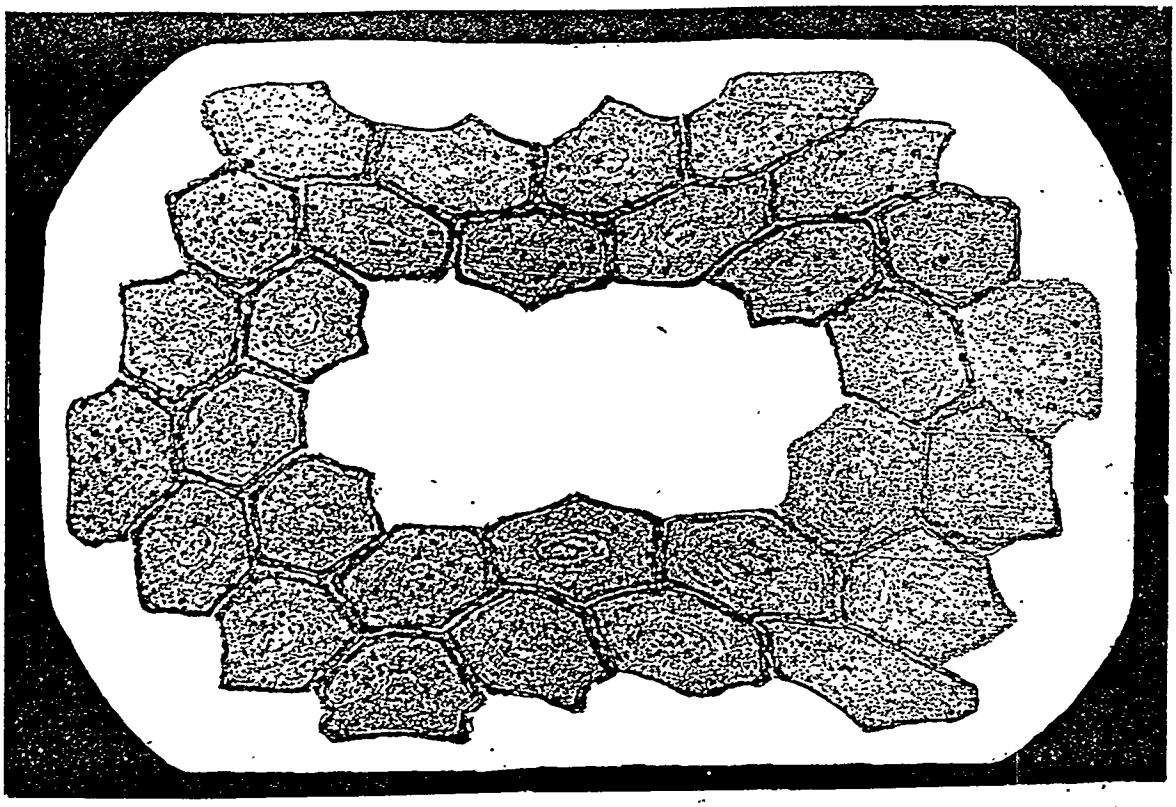

2330 HC

c

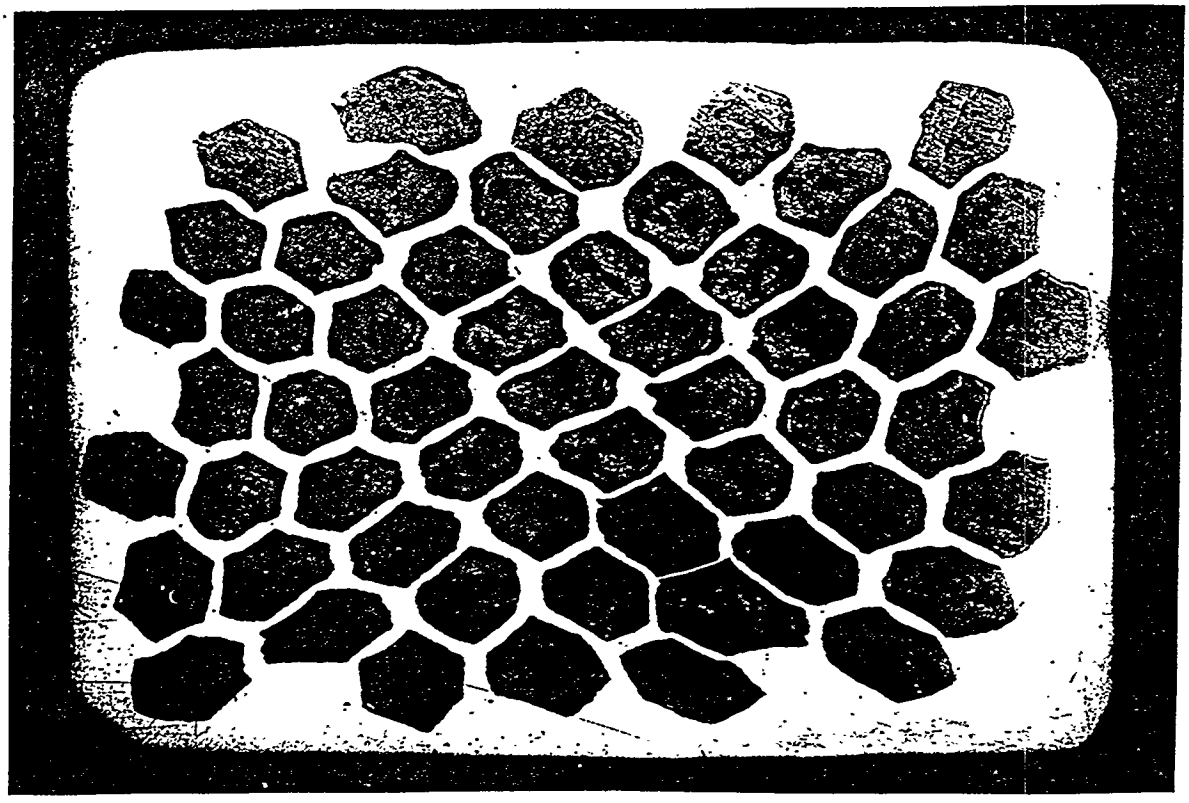

2355 NHC

d

Fig. 12

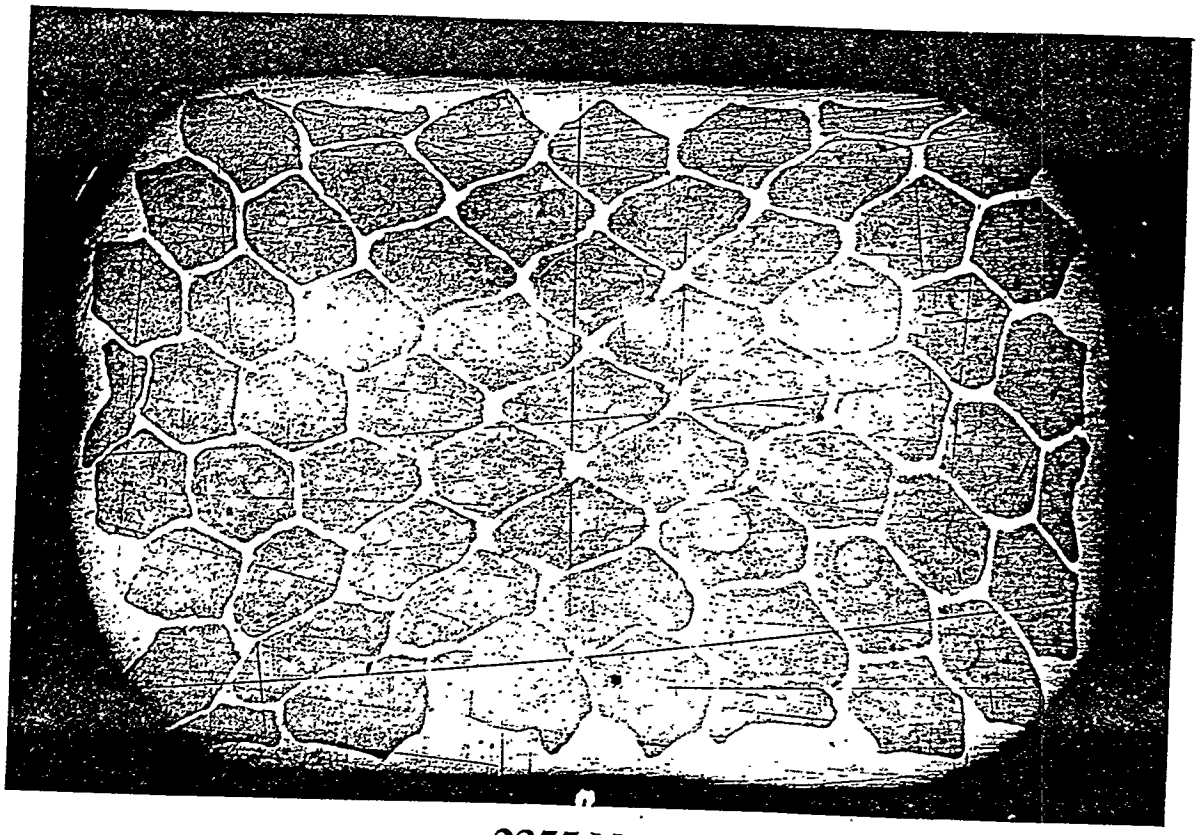

2355 N e

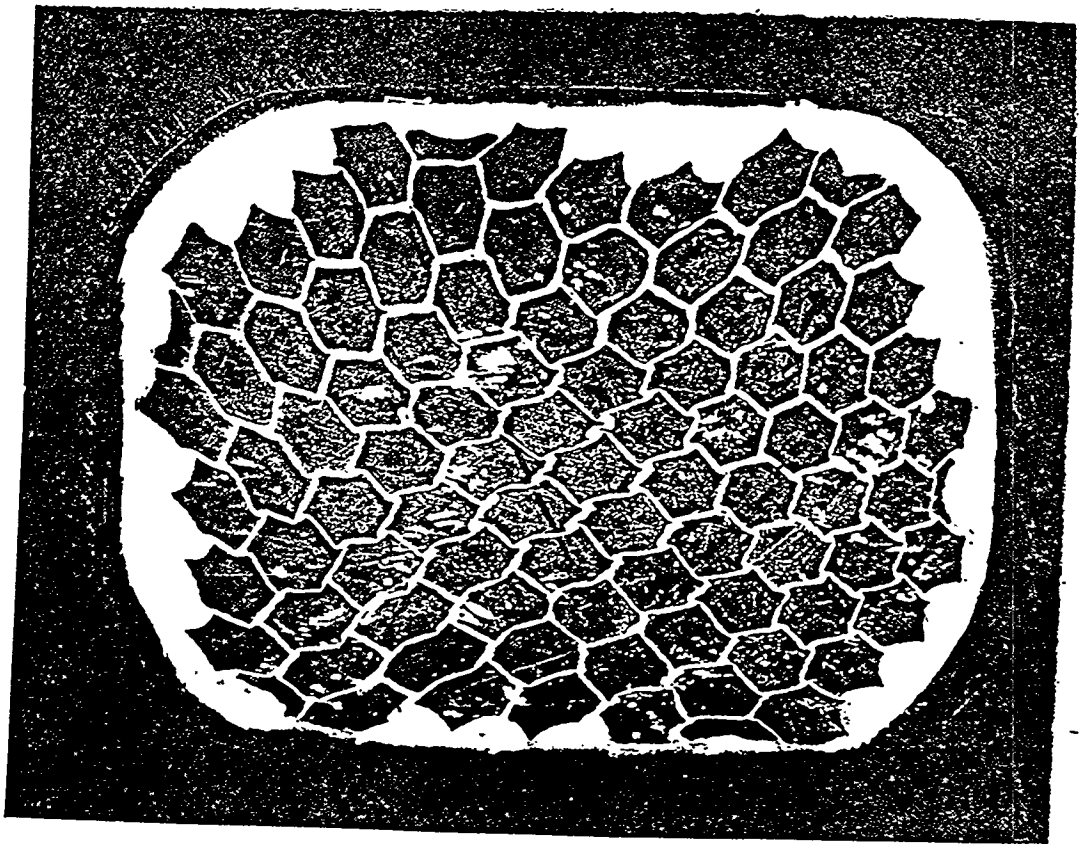

3485 N f

Fig. 12

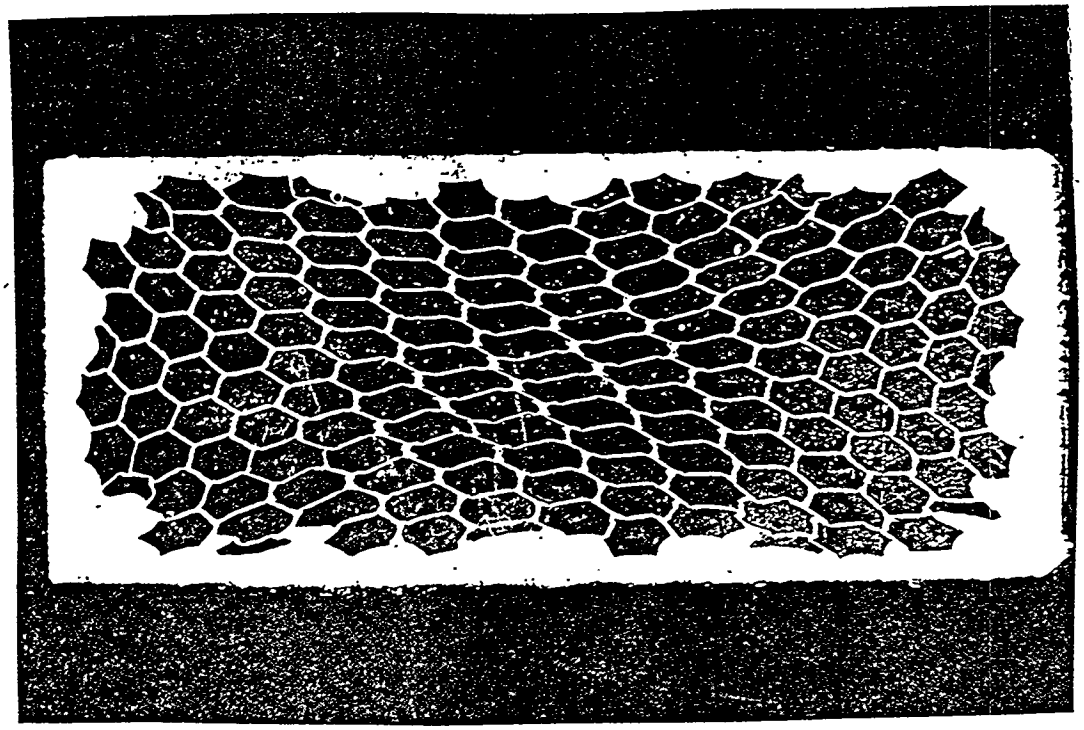

37139 N

CHARACTERISTICS OF Cu - Nb WIRES

Type	Dimensions, mm	UTS, MPa	YS, MPa	% IACS	RRR 77
2337	2 x 3	910	690	70	4.4
2336	2 x 3	1080	725	67	4.9
2330 HC	2 x 3	950	595	74	5.3
2355 NHC	2 x 3	1050	710	75	5.7
2385 N	2 x 3	1130	850	72	4.9
3485 N	3 x 4	1020	650	70	4.8
37139 N	3 x 7	1000	620	70	5.0

Fig. 12

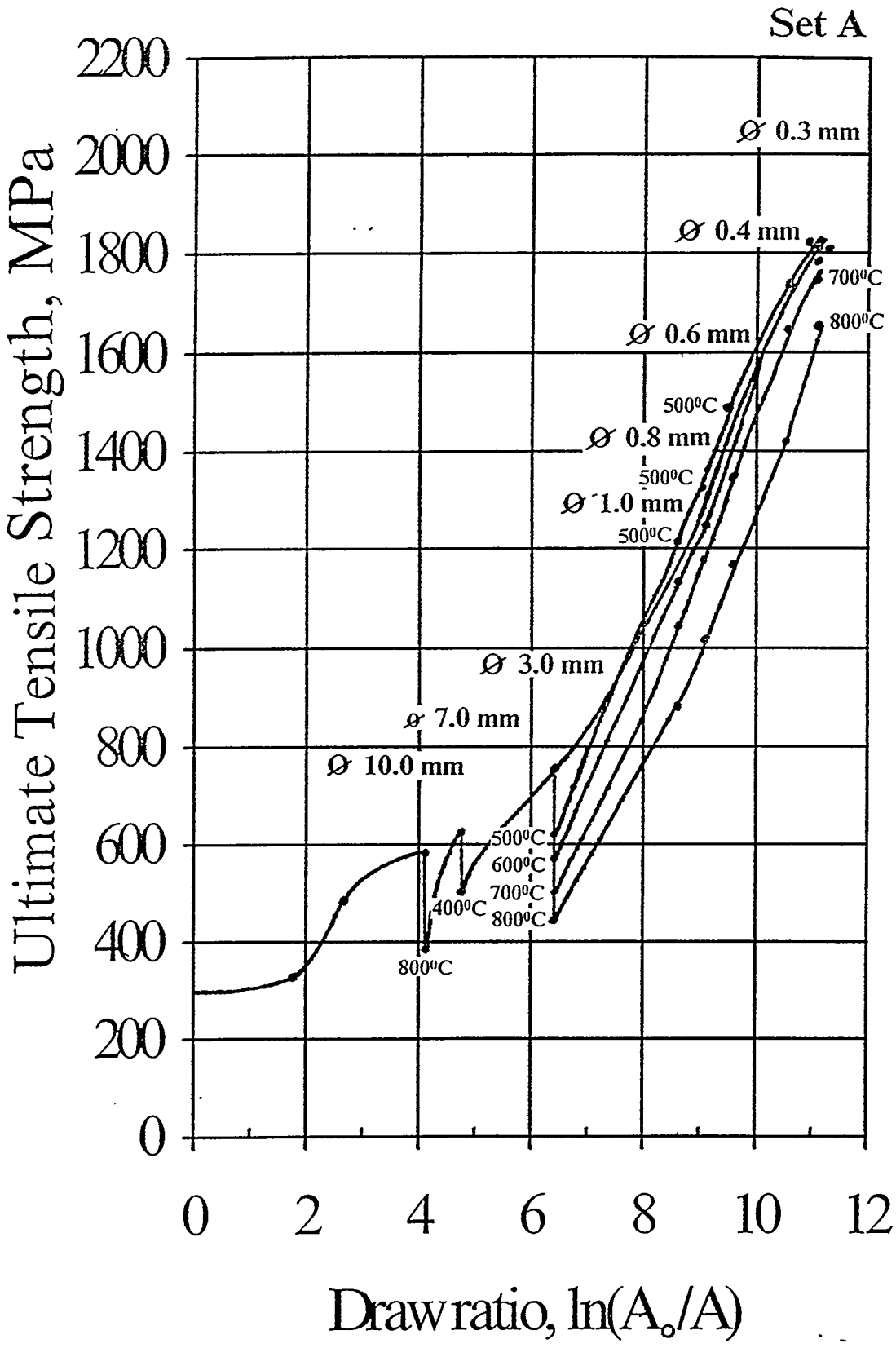
Set A
Ultimate Tensile Strength, MPa
2200
2000
1800
1600
1400
1200
1000
800
600
400
200
0
0
2
4
6
8
10
12
Draw ratio, ln(A$_o$/A)
Ø 0.3 mm
Ø 0.4 mm
Ø 0.6 mm
Ø 0.8 mm
Ø 1.0 mm
Ø 3.0 mm
Ø 7.0 mm
Ø 10.0 mm
500°C
600°C
700°C
800°C
400°C

Fig. 9 a

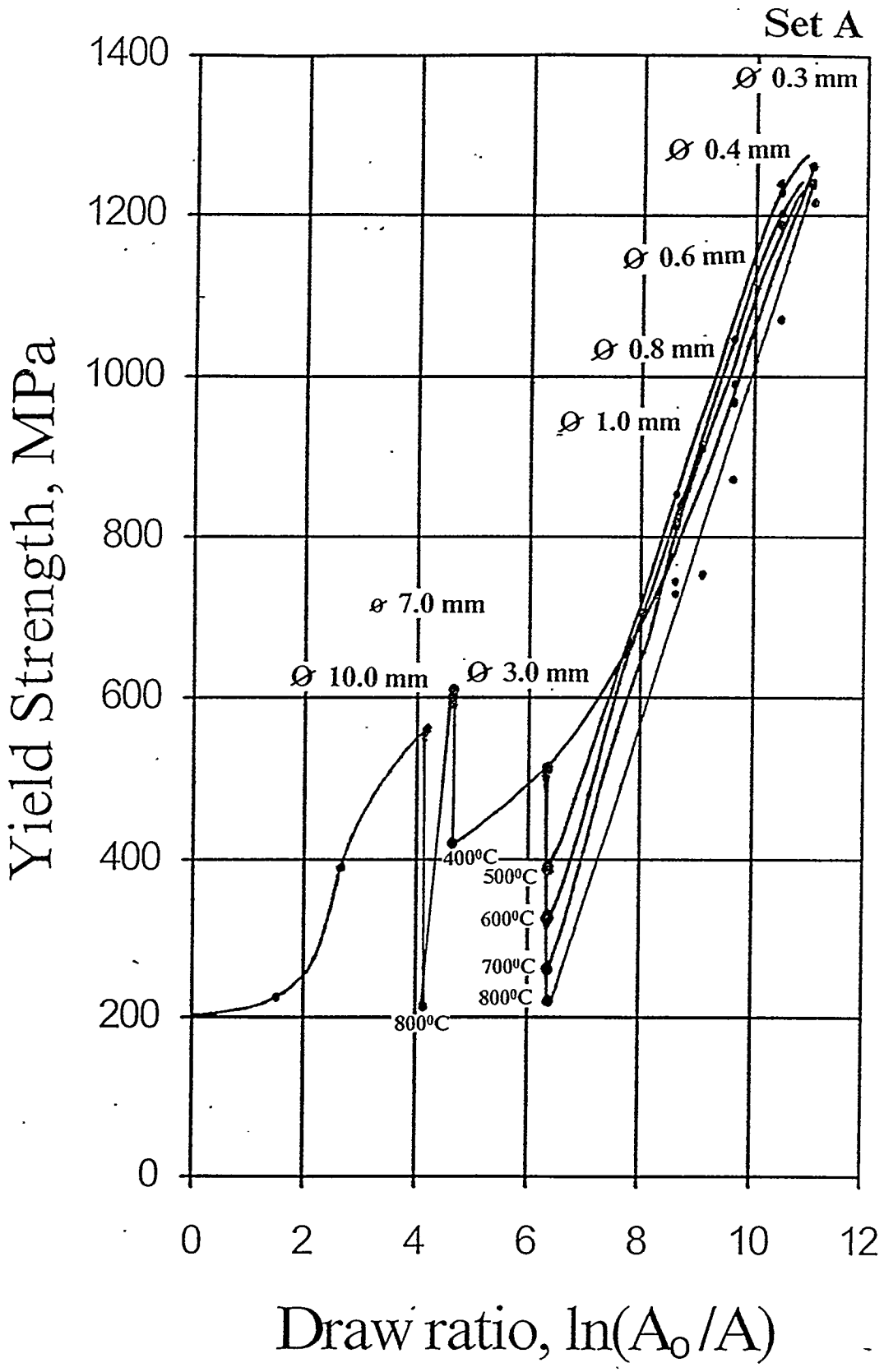
Set A
Ø 0.3 mm
Ø 0.4 mm
Ø 0.6 mm
Ø 0.8 mm
Ø 1.0 mm
Ø 3.0 mm
Ø 7.0 mm
Ø 10.0 mm
400°C
500°C
600°C
700°C
800°C
800°C
Yield Strength, MPa
Draw ratio, ln(A0/A)
0
200
400
600
800
1000
1200
1400
0
2
4
6
8
10
12

Fig. 9 b

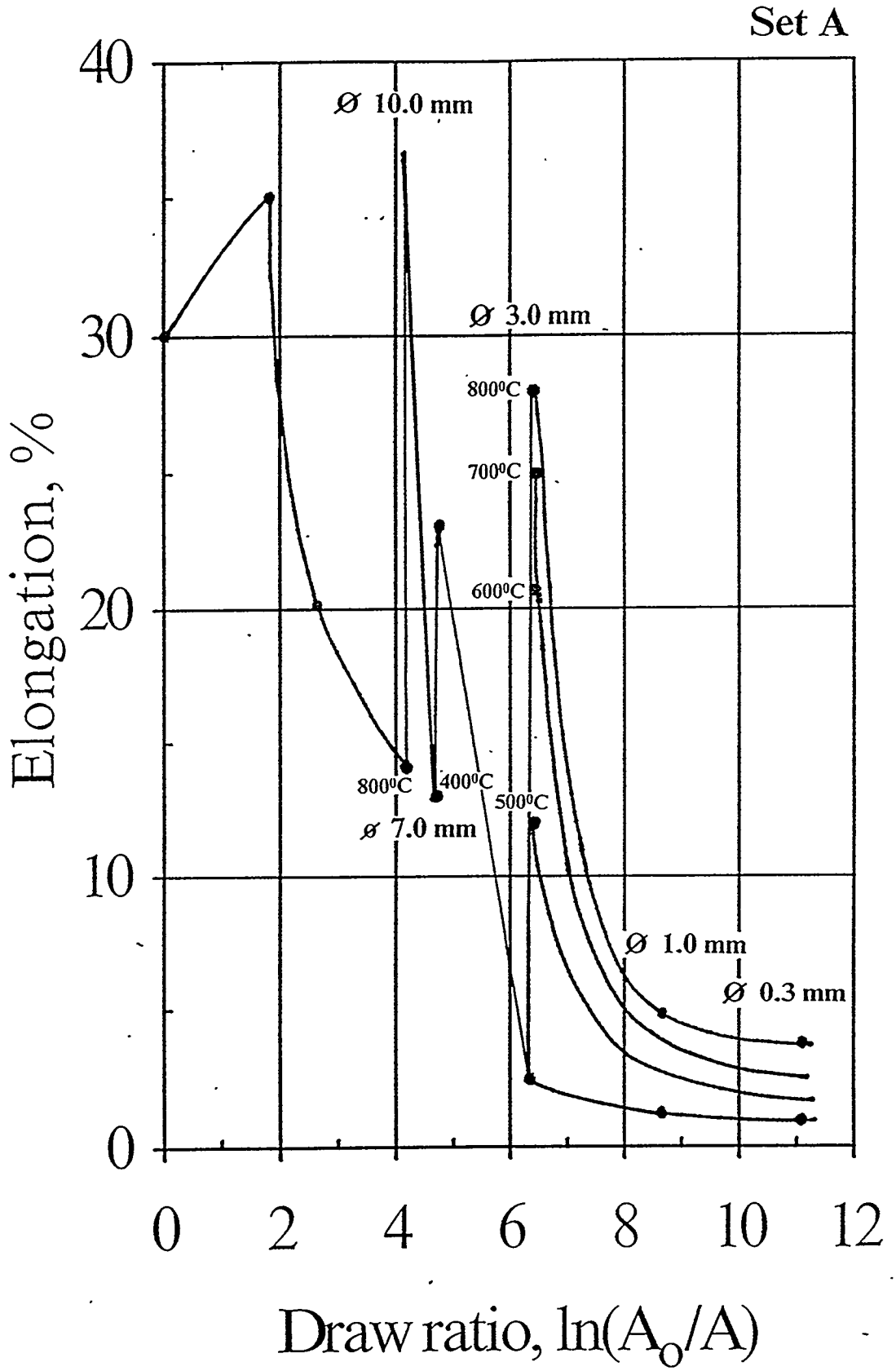
Set A
40
30
20
10
0
Elongation, %
Ø 10.0 mm
Ø 3.0 mm
800°C
700°C
600°C
800°C
400°C
500°C
ø 7.0 mm
Ø 1.0 mm
Ø 0.3 mm
0
2
4
6
8
10
12
Draw ratio, ln(A0/A)

Fig. 9 c

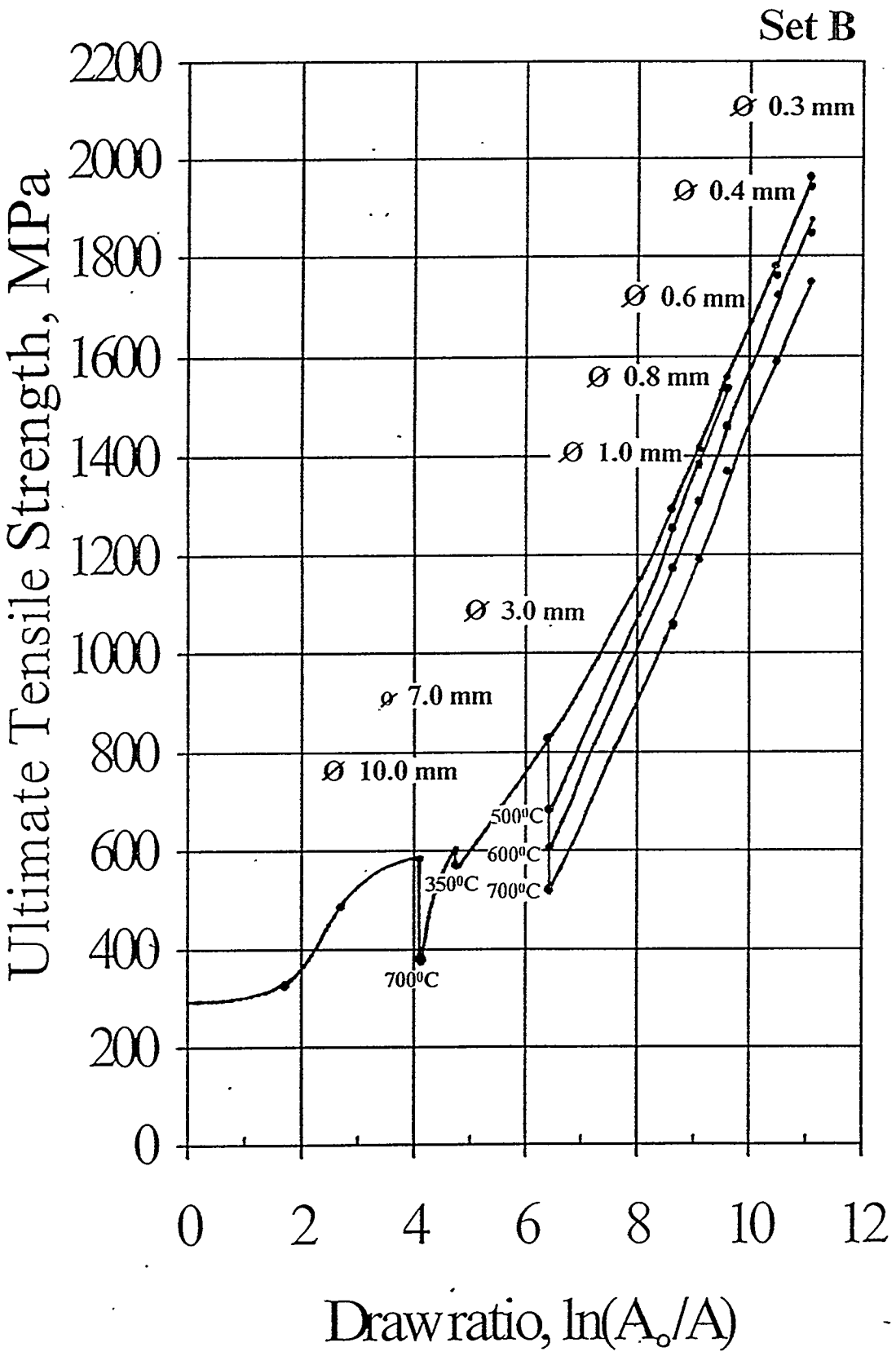
Set B
Ultimate Tensile Strength, MPa
2200
2000
1800
1600
1400
1200
1000
800
600
400
200
0
0
2
4
6
8
10
12
Draw ratio, ln(A$_o$/A)
Ø 0.3 mm
Ø 0.4 mm
Ø 0.6 mm
Ø 0.8 mm
Ø 1.0 mm
Ø 3.0 mm
Ø 7.0 mm
Ø 10.0 mm
500°C
600°C
700°C
350°C
700°C

Fig 9 d

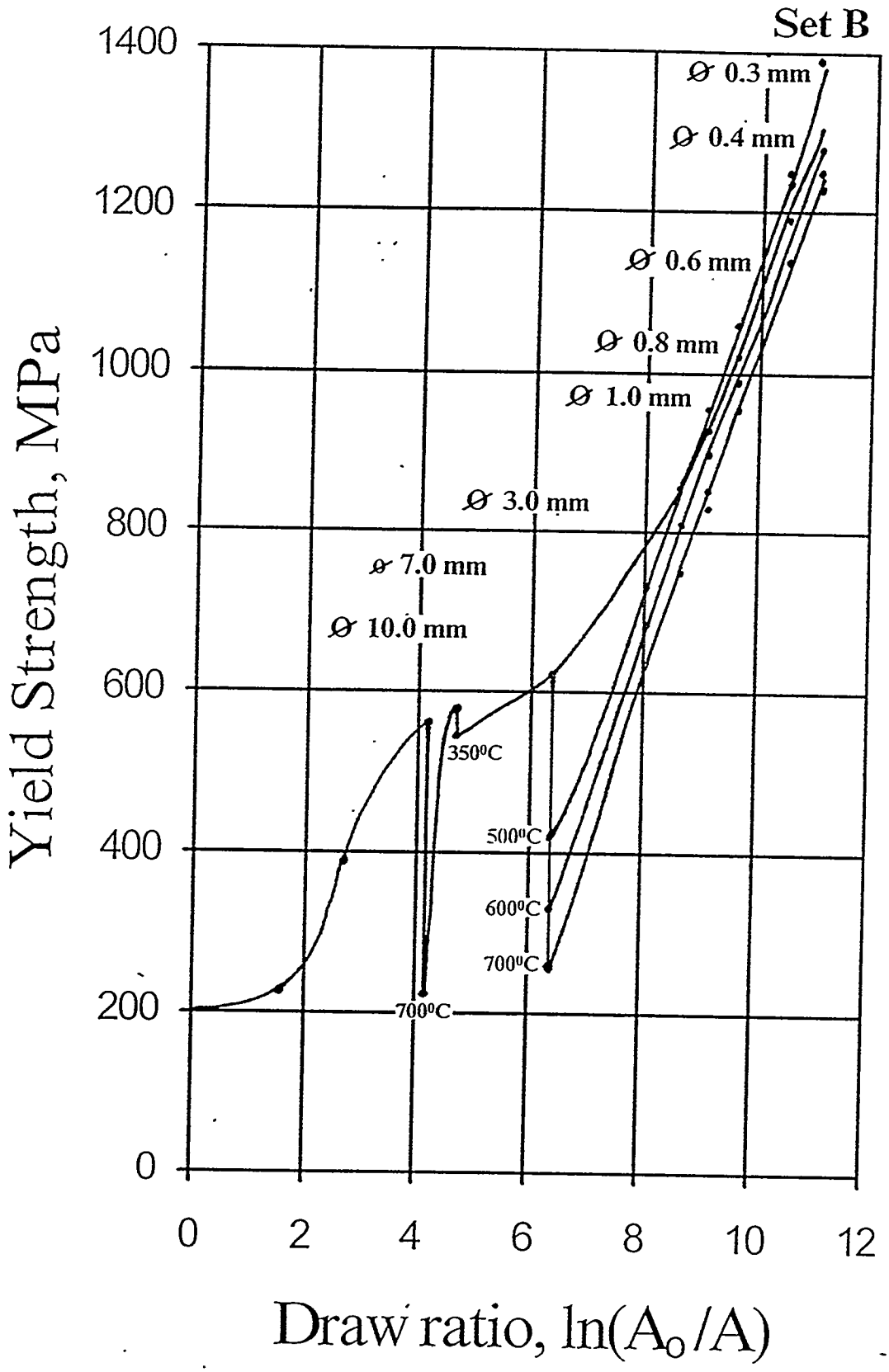
Set B
1400
1200
1000
800
600
400
200
0
0
2
4
6
8
10
12
Yield Strength, MPa
Draw ratio, ln(A0/A)
Ø 0.3 mm
Ø 0.4 mm
Ø 0.6 mm
Ø 0.8 mm
Ø 1.0 mm
Ø 3.0 mm
Ø 7.0 mm
Ø 10.0 mm
350°C
500°C
600°C
700°C
700°C

Fig. 9 e

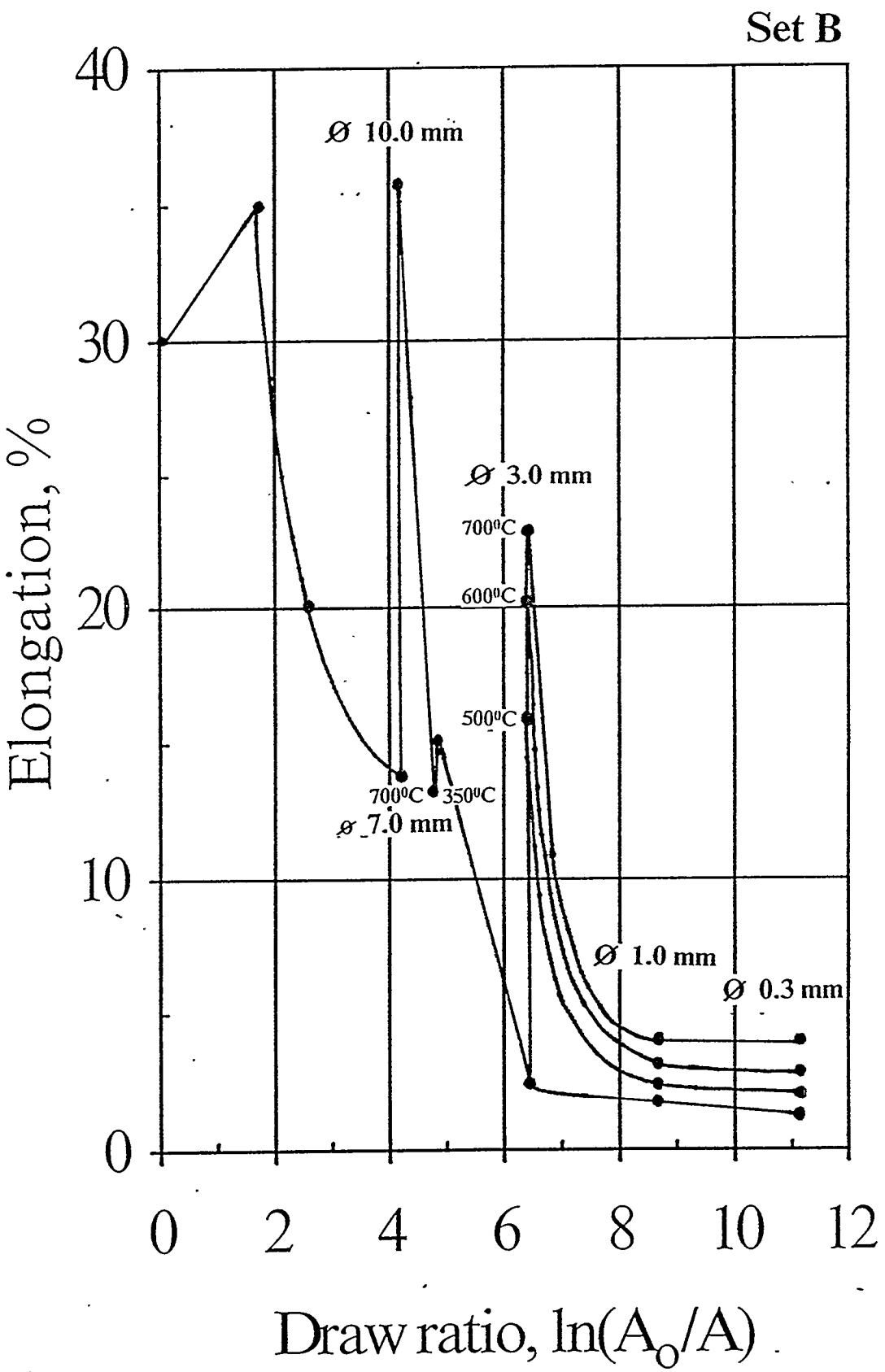
Set B
40
30
20
10
0
Elongation, %
Ø 10.0 mm
Ø 3.0 mm
700°C
600°C
500°C
700°C
350°C
Ø 7.0 mm
Ø 1.0 mm
Ø 0.3 mm
0
2
4
6
8
10
12
Draw ratio, ln(A0/A)

Fig. 9 f

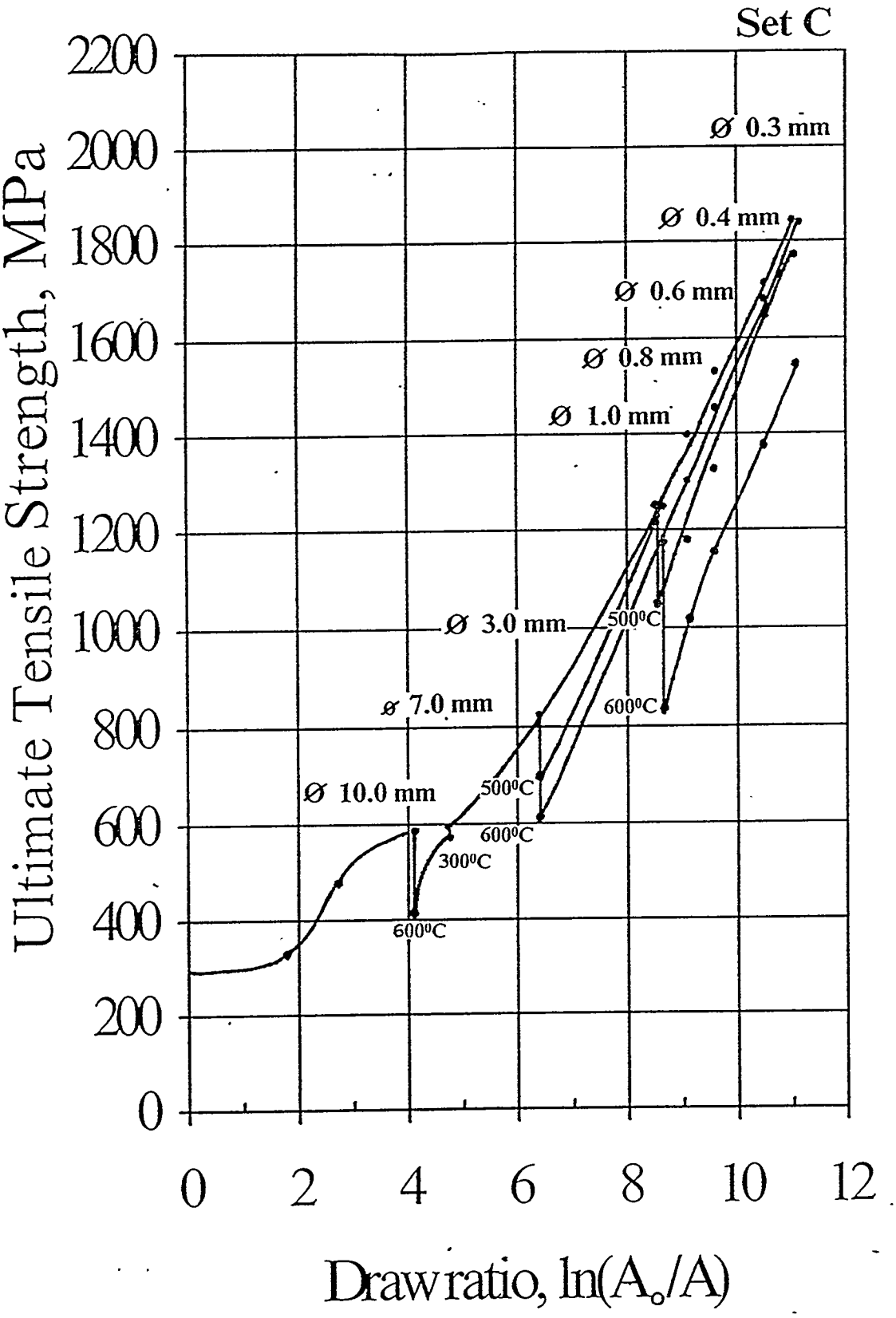
Set C
Ultimate Tensile Strength, MPa
2200
2000
1800
1600
1400
1200
1000
800
600
400
200
0
0
2
4
6
8
10
12
Draw ratio, ln(A₀/A)
Ø 0.3 mm
Ø 0.4 mm
Ø 0.6 mm
Ø 0.8 mm
Ø 1.0 mm
Ø 3.0 mm
ø 7.0 mm
Ø 10.0 mm
500°C
600°C
300°C
600°C
500°C
600°C

Fig 9 g

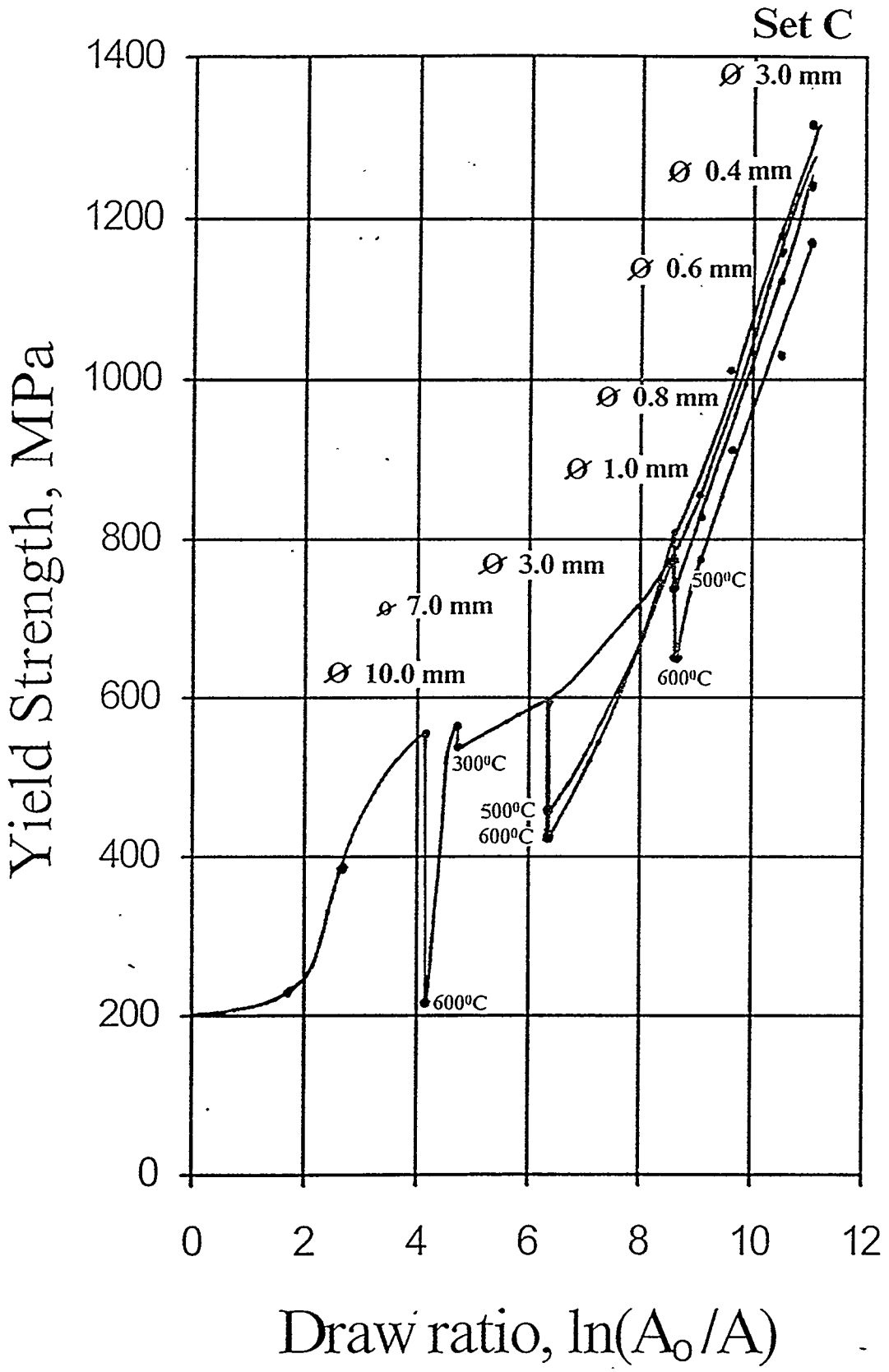
Set C
Yield Strength, MPa
Draw ratio, ln(A0/A)
1400
1200
1000
800
600
400
200
0
0
2
4
6
8
10
12
Ø 3.0 mm
Ø 0.4 mm
Ø 0.6 mm
Ø 0.8 mm
Ø 1.0 mm
Ø 3.0 mm
Ø 7.0 mm
Ø 10.0 mm
500°C
600°C
300°C
500°C
600°C
600°C

Fig 9 h

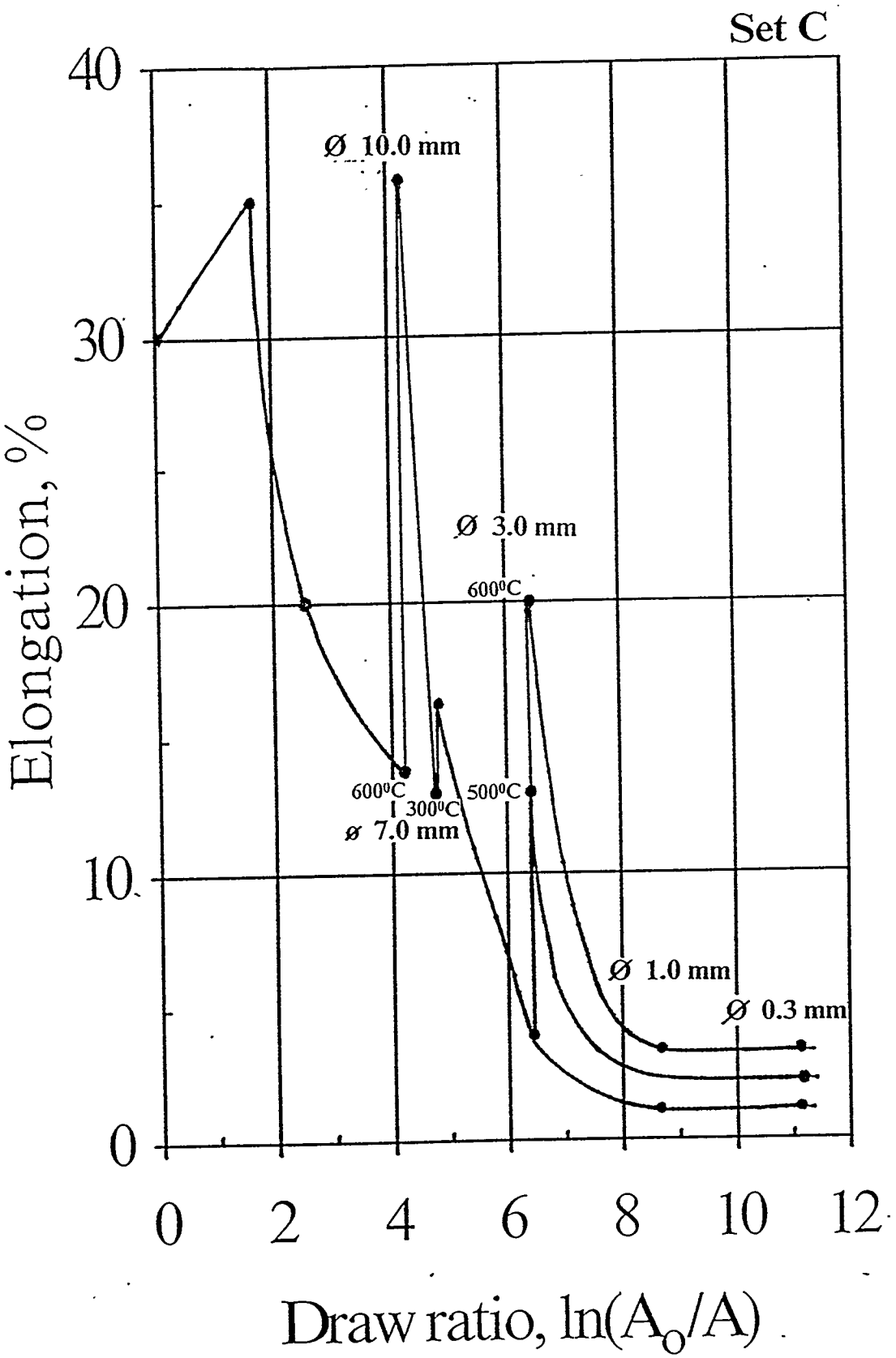
Set C
40
30
20
10
0
Elongation, %
Ø 10.0 mm
Ø 3.0 mm
600°C
600°C
300°C
ø 7.0 mm
500°C
Ø 1.0 mm
Ø 0.3 mm
0
2
4
6
8
10
12
Draw ratio, ln(A0/A)

Fig. 9 i

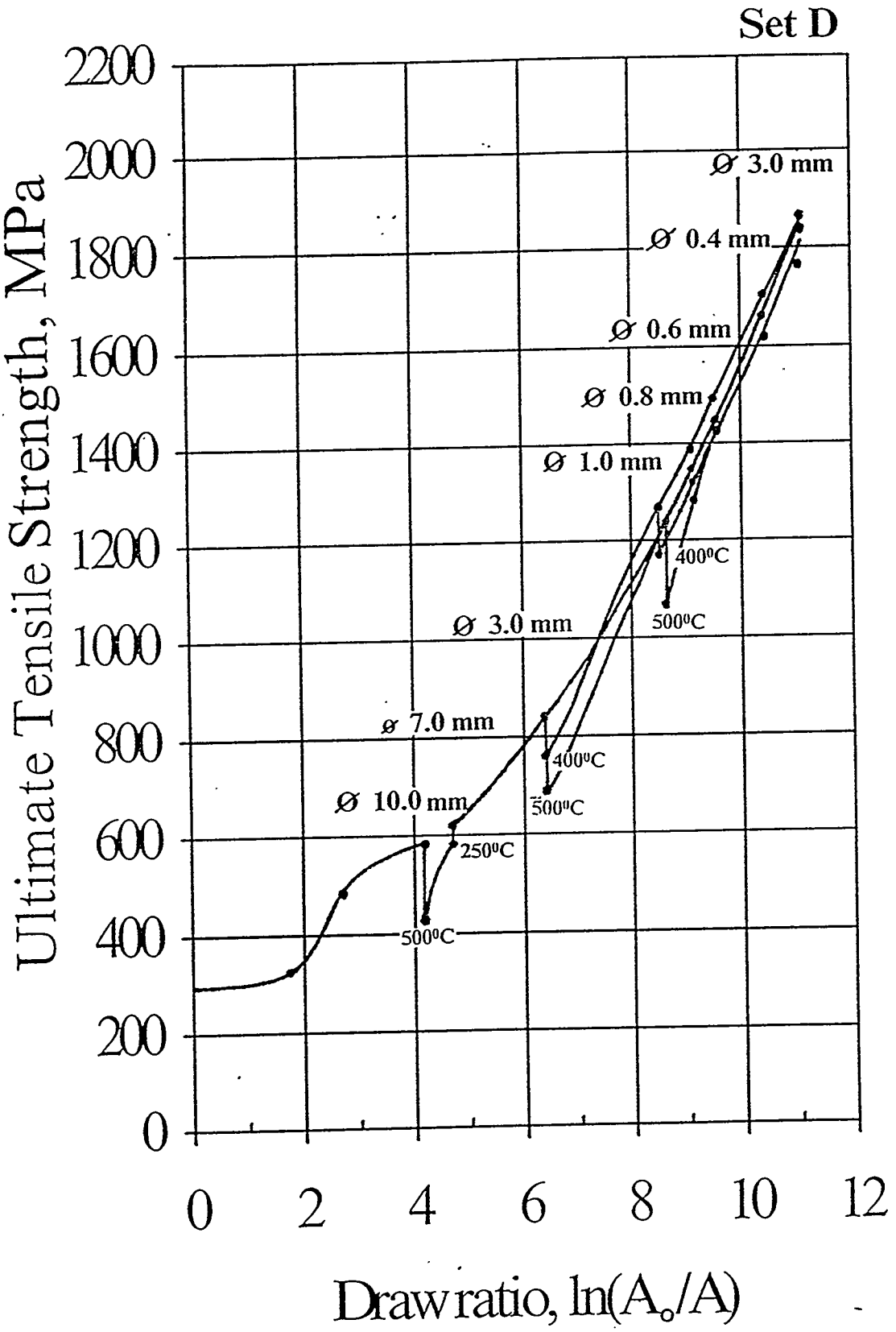
Set D
Ultimate Tensile Strength, MPa
2200
2000
1800
1600
1400
1200
1000
800
600
400
200
0
0
2
4
6
8
10
12
Draw ratio, ln(A₀/A)
Ø 3.0 mm
Ø 0.4 mm
Ø 0.6 mm
Ø 0.8 mm
Ø 1.0 mm
400°C
500°C
Ø 3.0 mm
Ø 7.0 mm
400°C
500°C
Ø 10.0 mm
250°C
500°C

Fig. 9 j

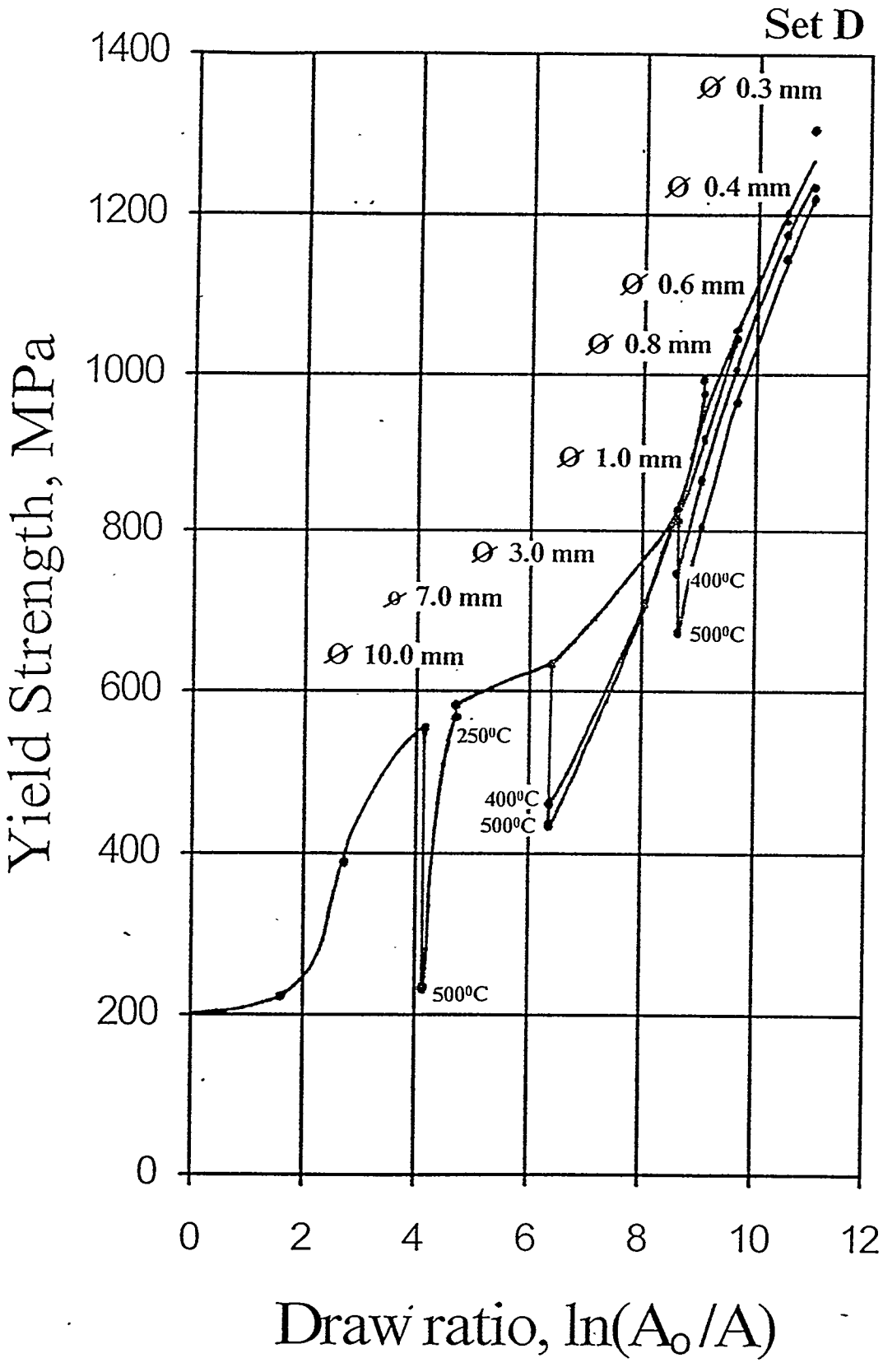
Set D
Yield Strength, MPa
Draw ratio, ln(A0/A)
1400
1200
1000
800
600
400
200
0
0
2
4
6
8
10
12
Ø 0.3 mm
Ø 0.4 mm
Ø 0.6 mm
Ø 0.8 mm
Ø 1.0 mm
Ø 3.0 mm
Ø 7.0 mm
Ø 10.0 mm
400°C
500°C
250°C
400°C
500°C
500°C

Fig 9 k

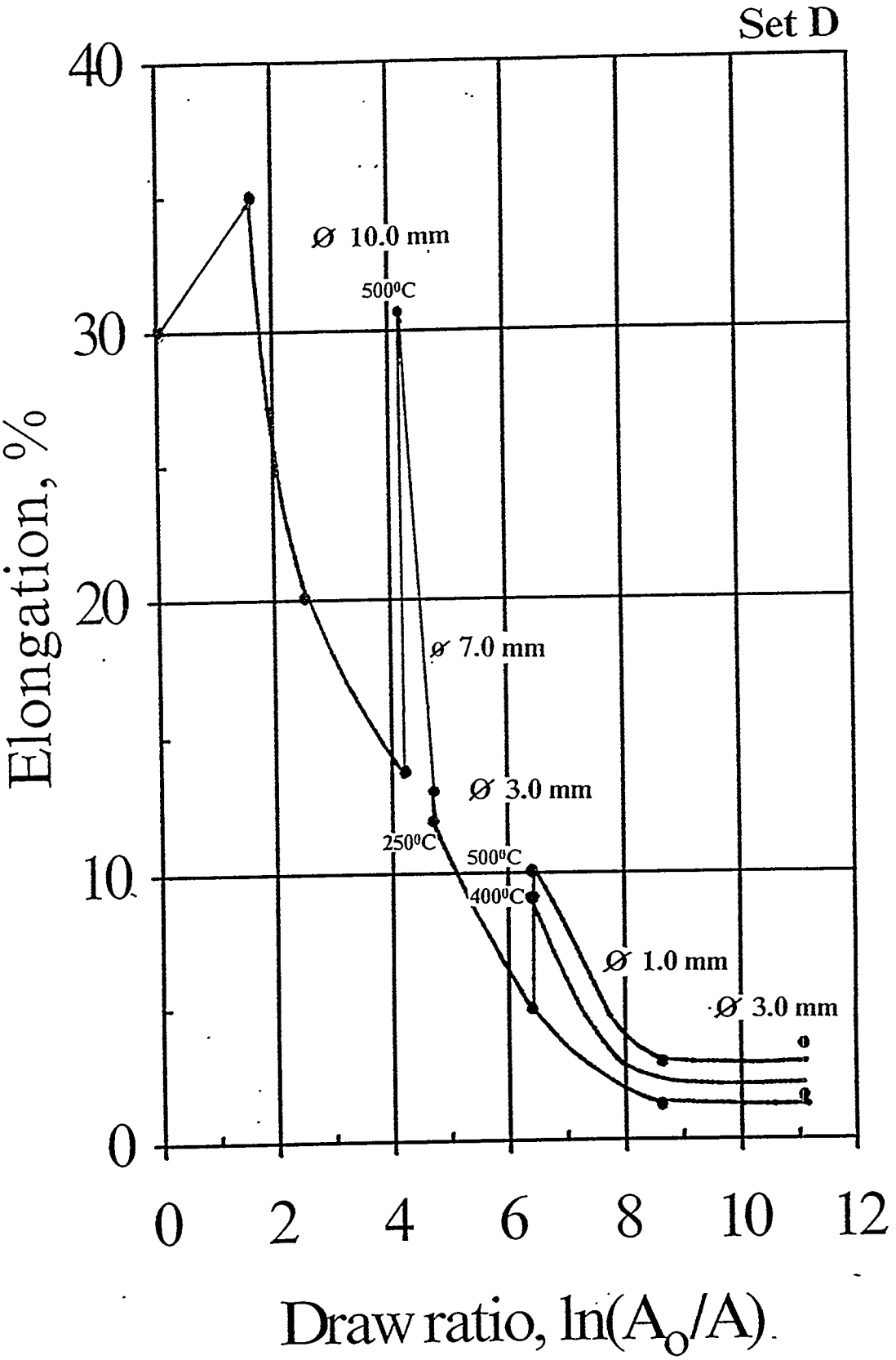
Set D
40
30
20
10
0
Elongation, %
Ø 10.0 mm
500°C
Ø 7.0 mm
Ø 3.0 mm
250°C
500°C
400°C
Ø 1.0 mm
Ø 3.0 mm
0
2
4
6
8
10
12
Draw ratio, ln(A0/A)

Fig. 3 l

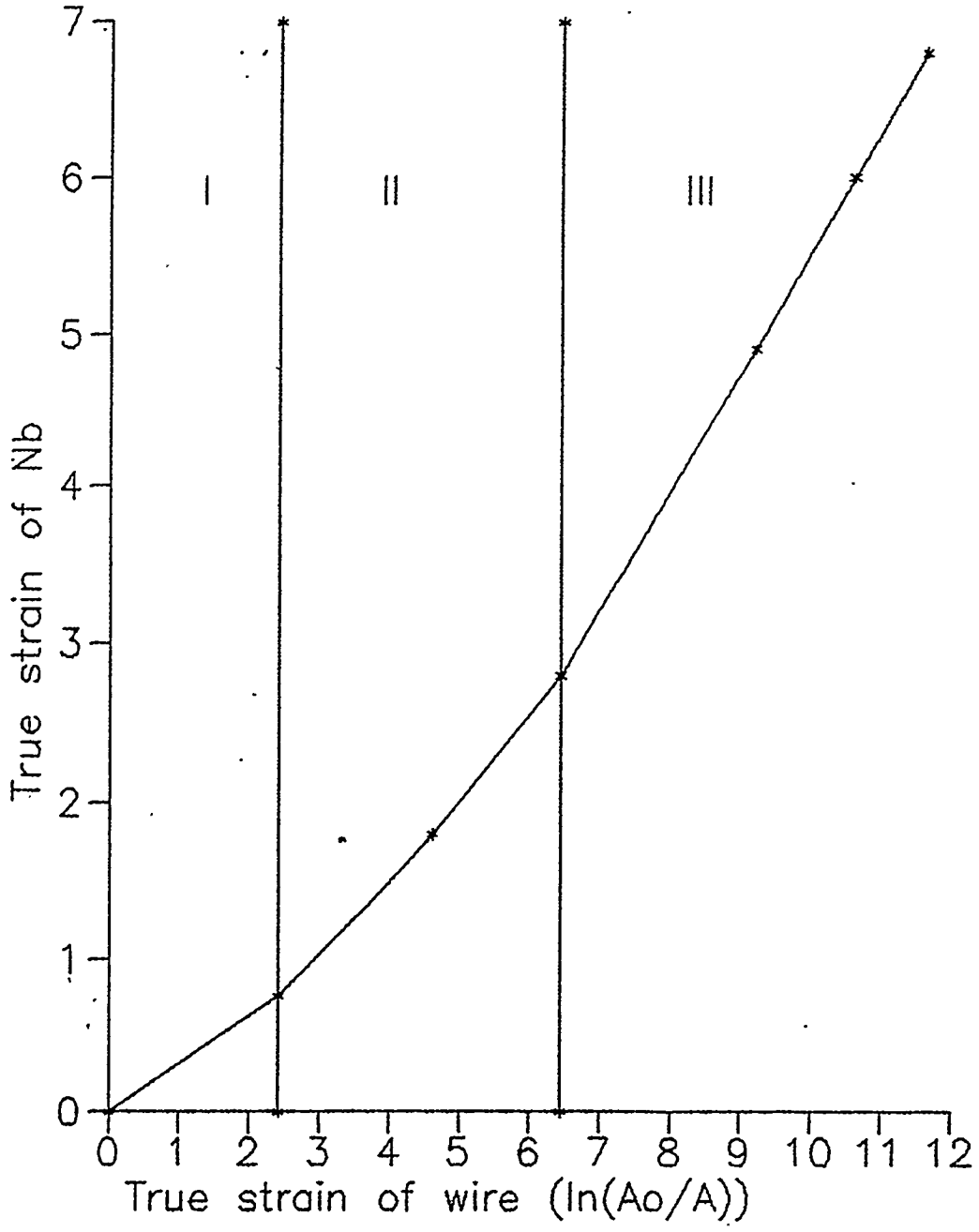
True strain of Nb
True strain of wire (ln(Ao/A))
I
II
III
0
1
2
3
4
5
6
7
8
9
10
11
12

Fig 10

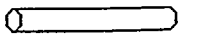

Nb rods

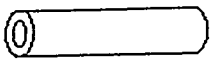

Cu tubes

etching
assembling

drawing

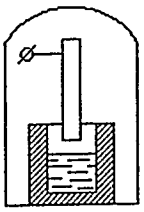

first
arc
melting

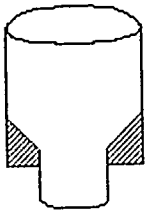

machining
extrusion

drawing

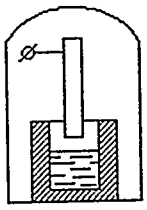

second
arc
melting

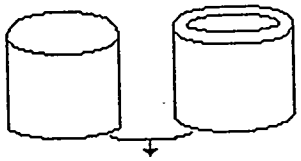

machining of
Cu-Nb ingot

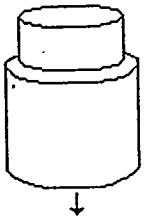

assembling
first
billet

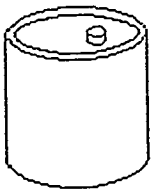

evacuating
welding

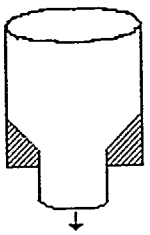

extrusion
of first
billet

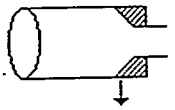

drawing
cutting
etching

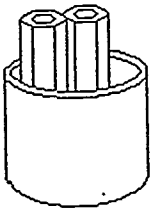

assembling
of second
billet

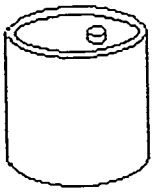

evacuating
welding

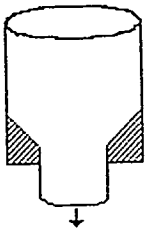

extrusion
of second
billet

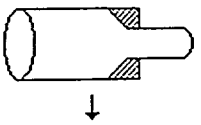

drawing with
intermediate
heat treatments

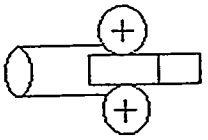

forming of the
final wire

TESTING - UTS, YS, %IACS, RRR

Fig 11

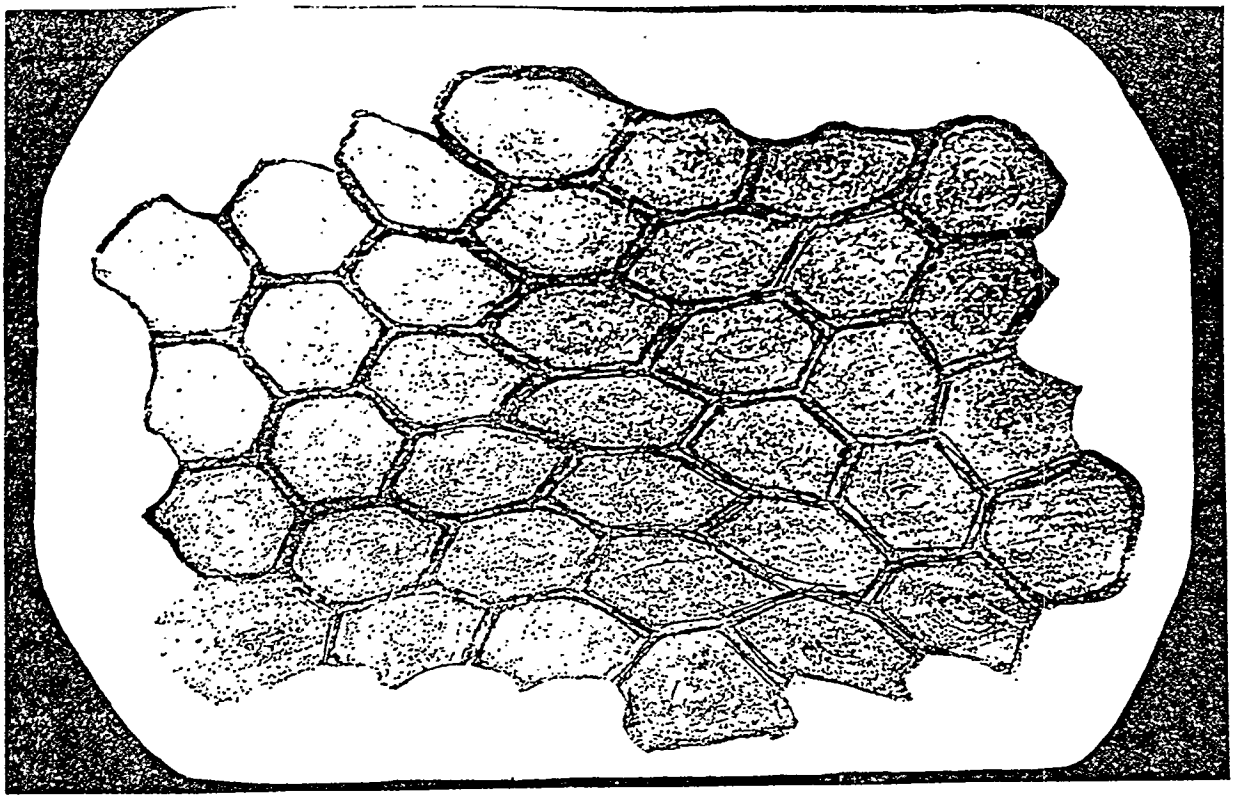

2337 a

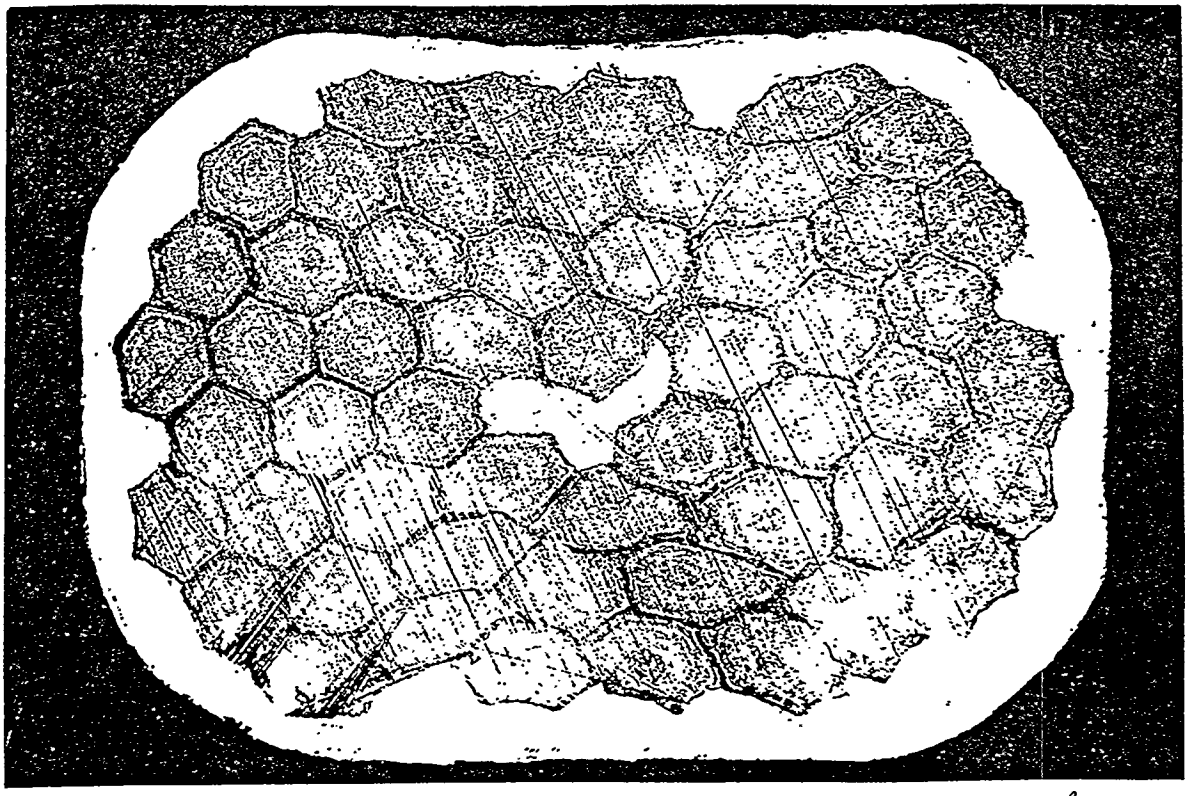

2354 b

Fig. 12

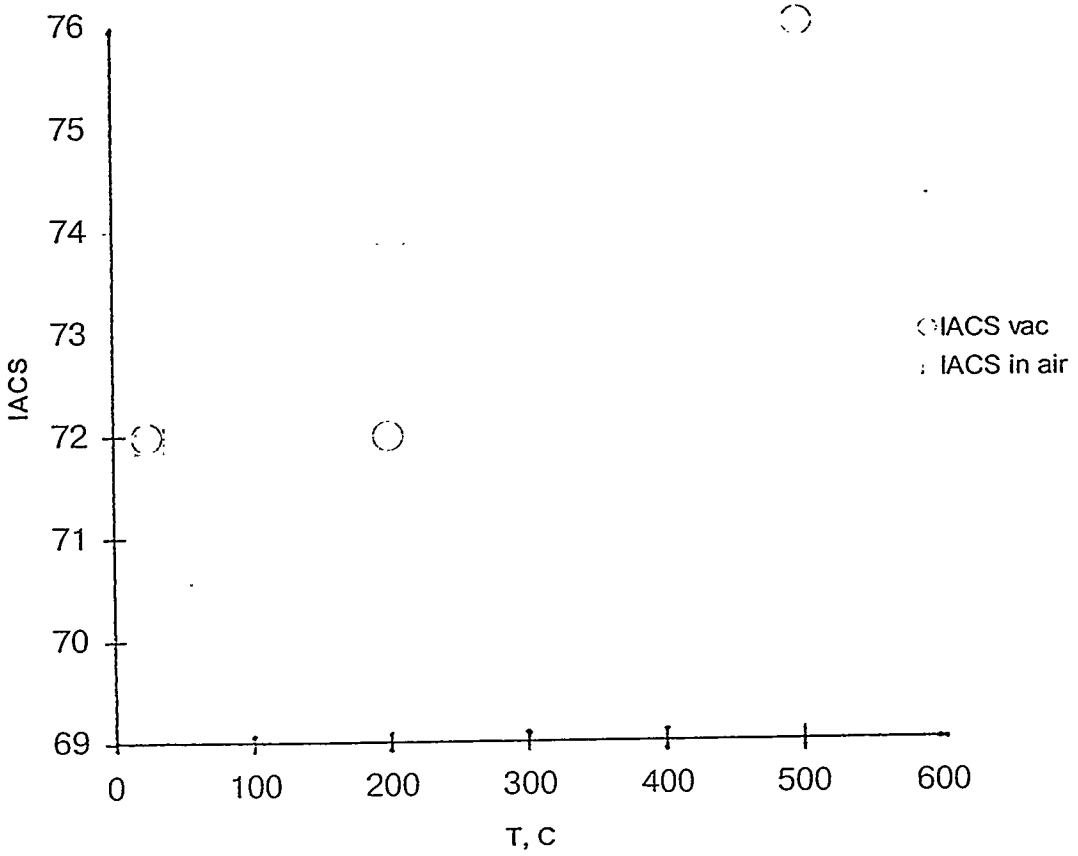
76
75
74
73
72
71
70
69
IACS
0
100
200
300
400
500
600
T, C
IACS vac
IACS in air

Fig. 13

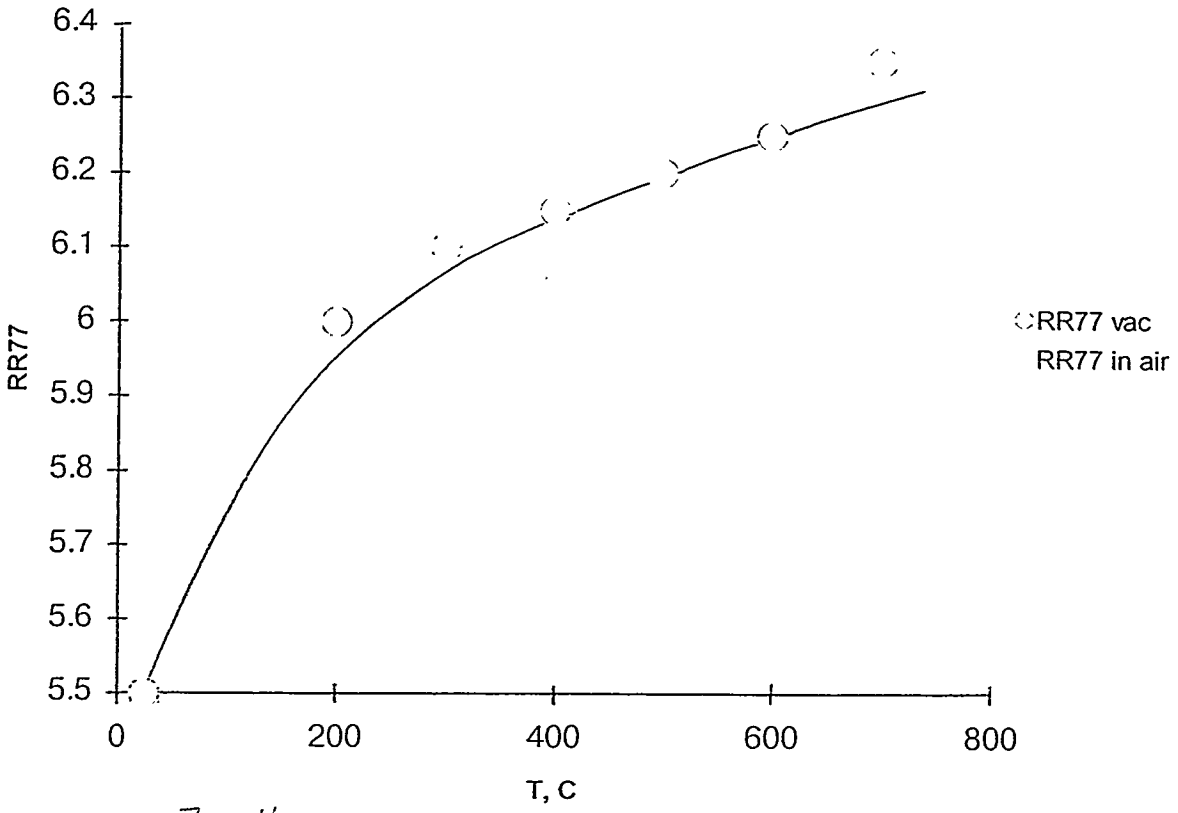
6.4
6.3
6.2
6.1
6
5.9
5.8
5.7
5.6
5.5
RR77
0
200
400
600
800
T, C
RR77 vac
RR77 in air

Fig 14

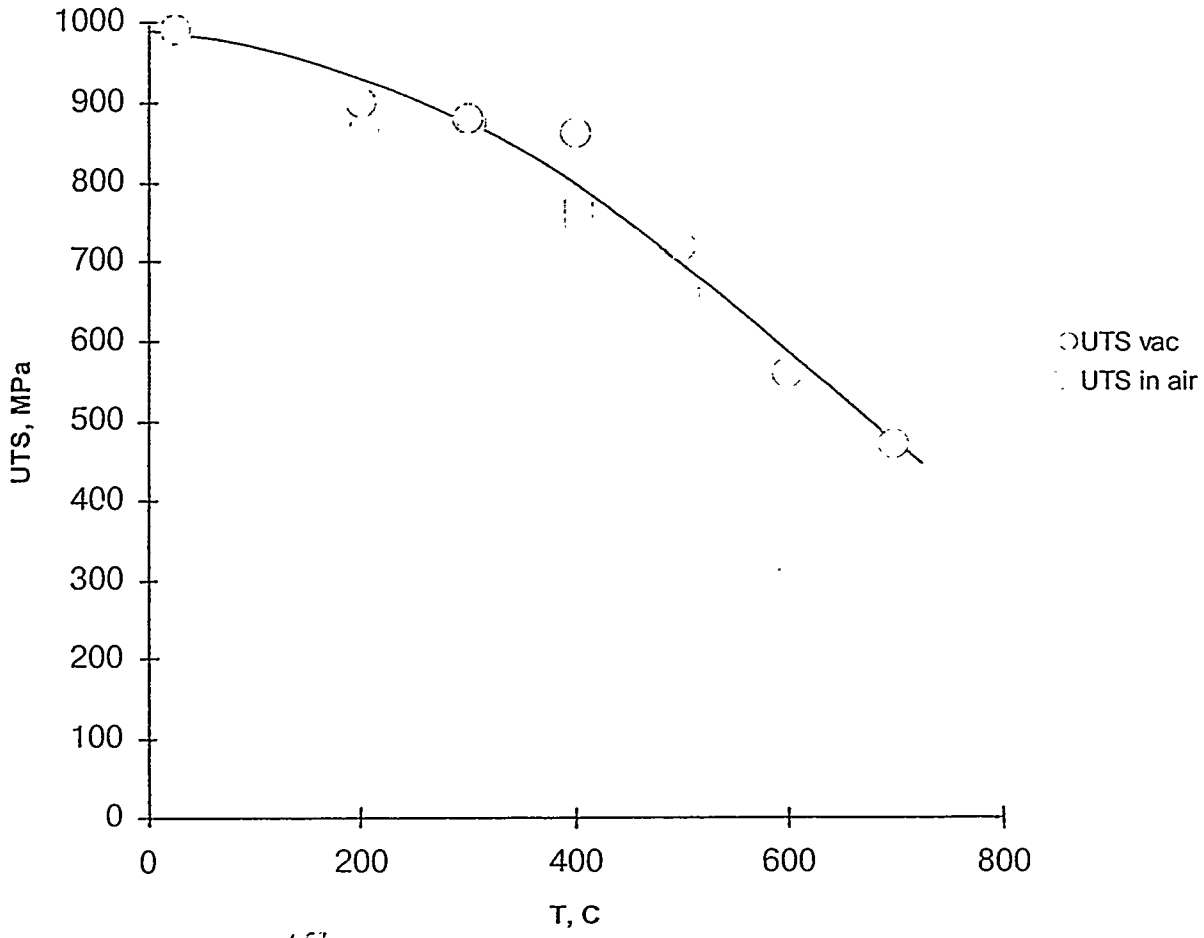
1000
900
800
700
600
500
400
300
200
100
0
UTS, MPa
0
200
400
600
800
T, C
UTS vac
UTS in air

Fig. 15 a

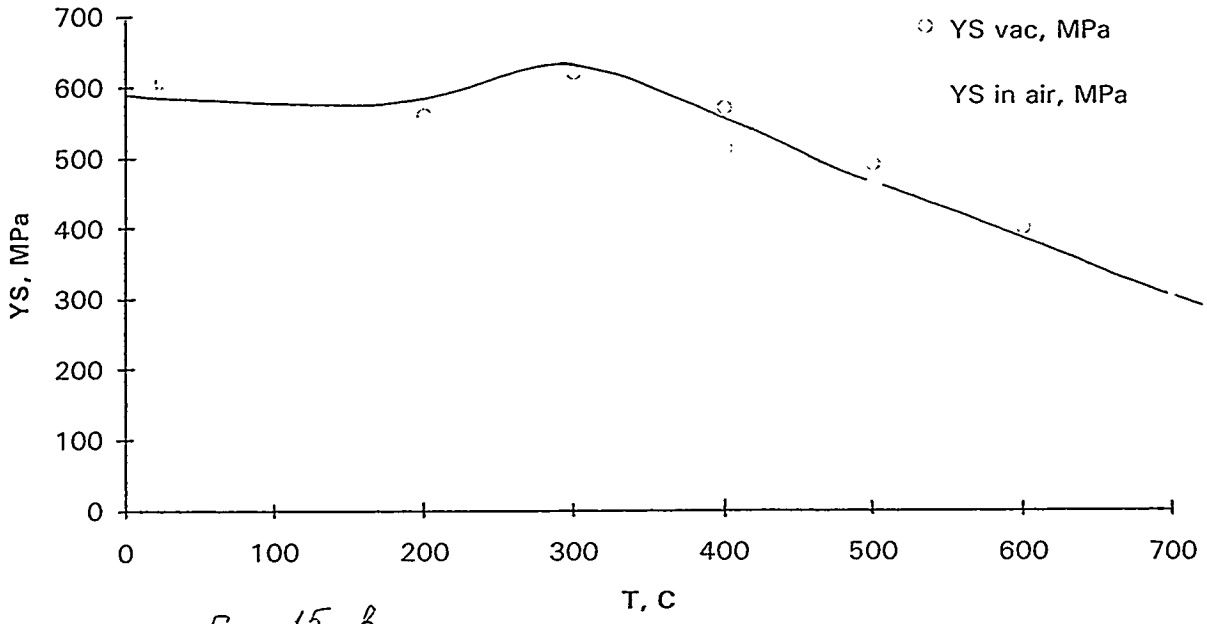
700
600
500
400
300
200
100
0
YS, MPa
0
100
200
300
400
500
600
700
T, C
YS vac, MPa
YS in air, MPa

Fig. 15 B

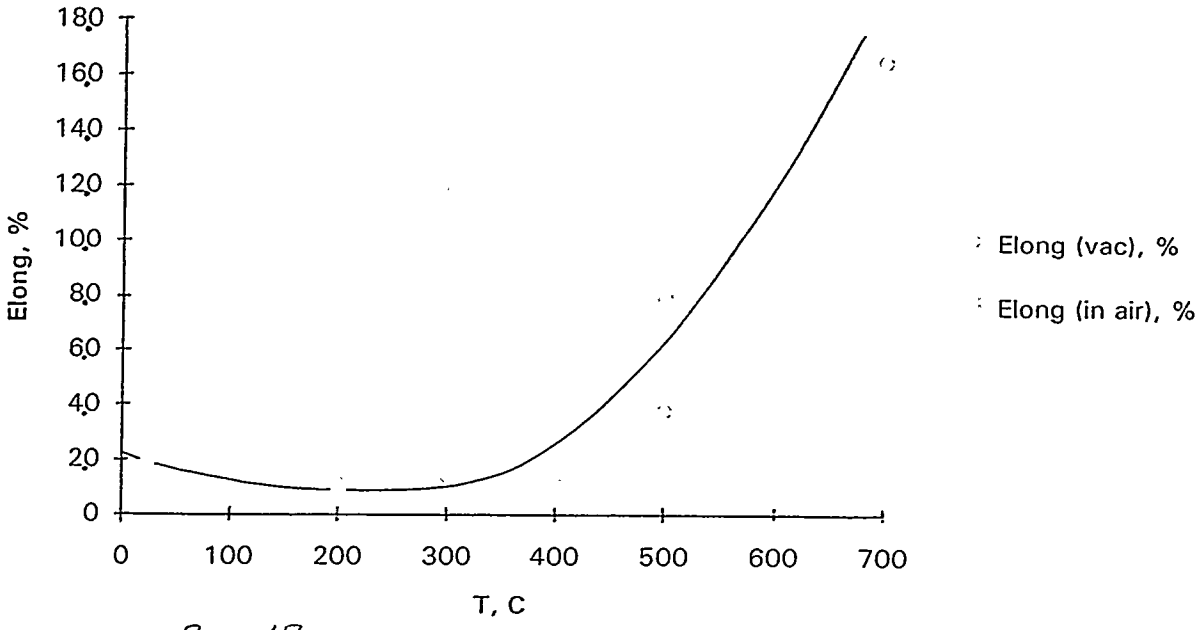
18.0
16.0
14.0
12.0
10.0
8.0
6.0
4.0
2.0
0
Elong, %
0
100
200
300
400
500
600
700
T, C
Elong (vac), %
Elong (in air), %

Fig. 15c

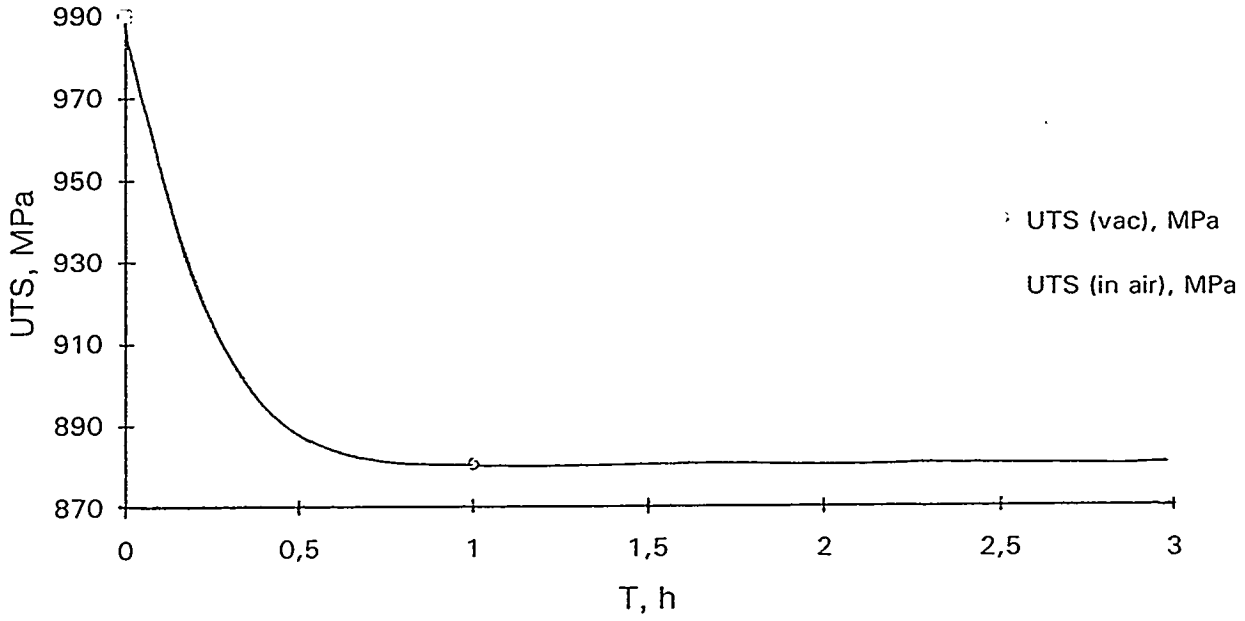
990
970
950
930
910
890
870
UTS, MPa
0
0,5
1
1,5
2
2,5
3
T, h
UTS (vac), MPa
UTS (in air), MPa

Fig 16 2

300°C

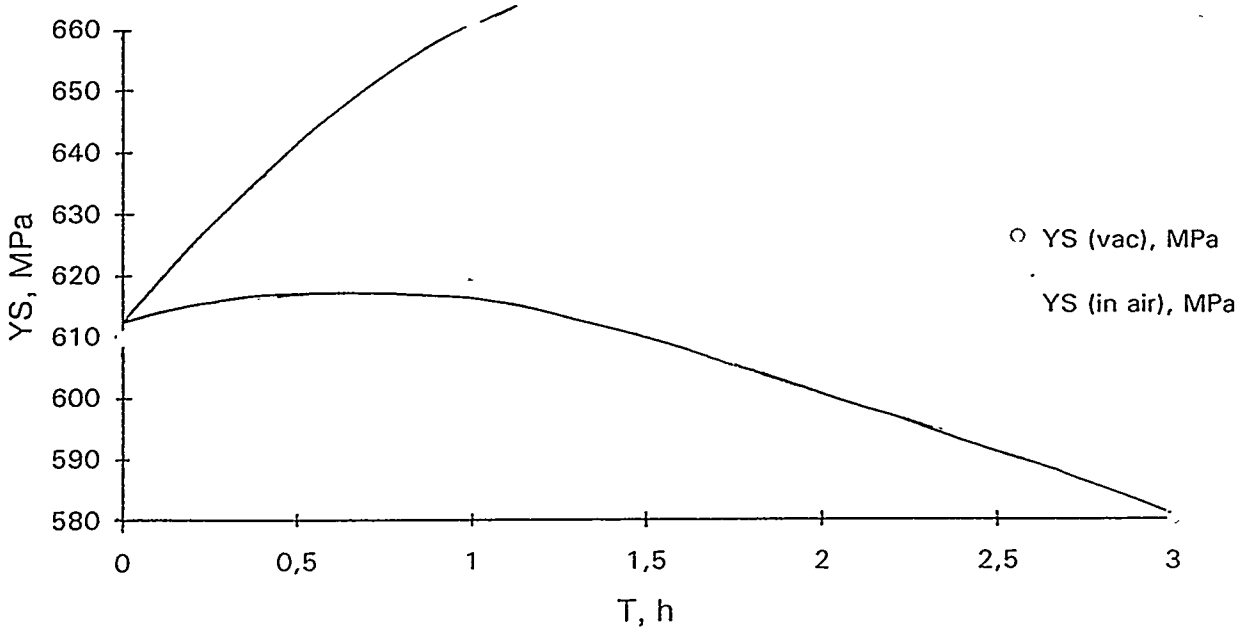
660
650
640
630
620
610
600
590
580
YS, MPa
0
0,5
1
1,5
2
2,5
3
T, h
YS (vac), MPa
YS (in air), MPa

Fig 16 b

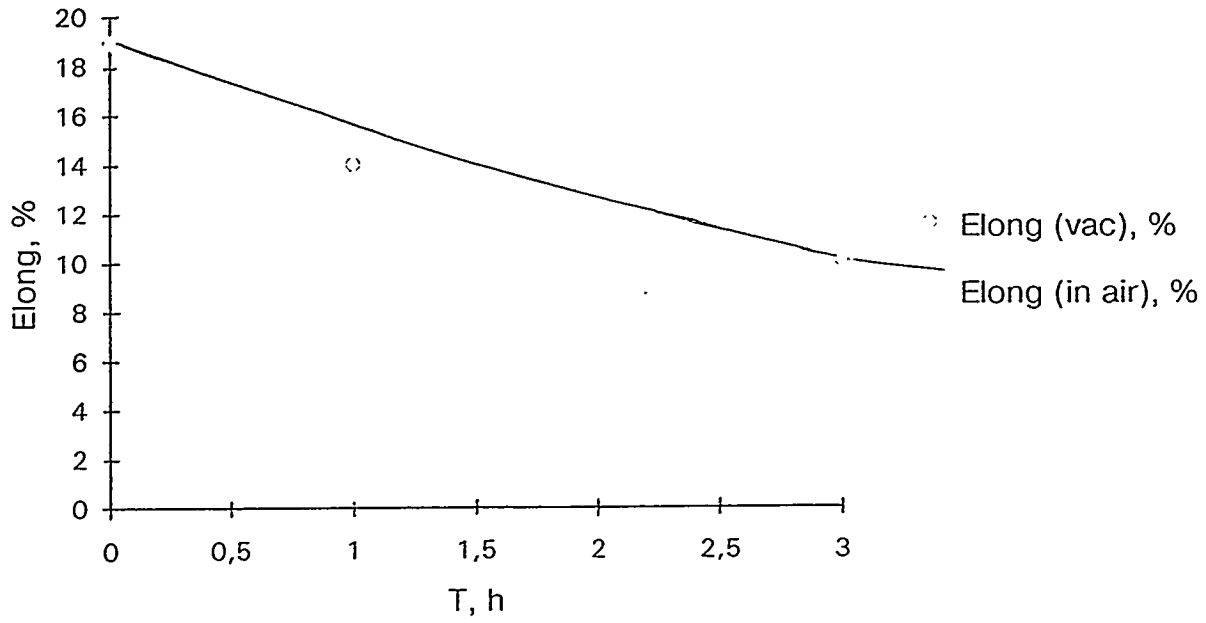
20
18
16
14
12
10
8
6
4
2
0
Elong, %
0
0,5
1
1,5
2
2,5
3
T, h
Elong (vac), %
Elong (in air), %

Fig 16 c

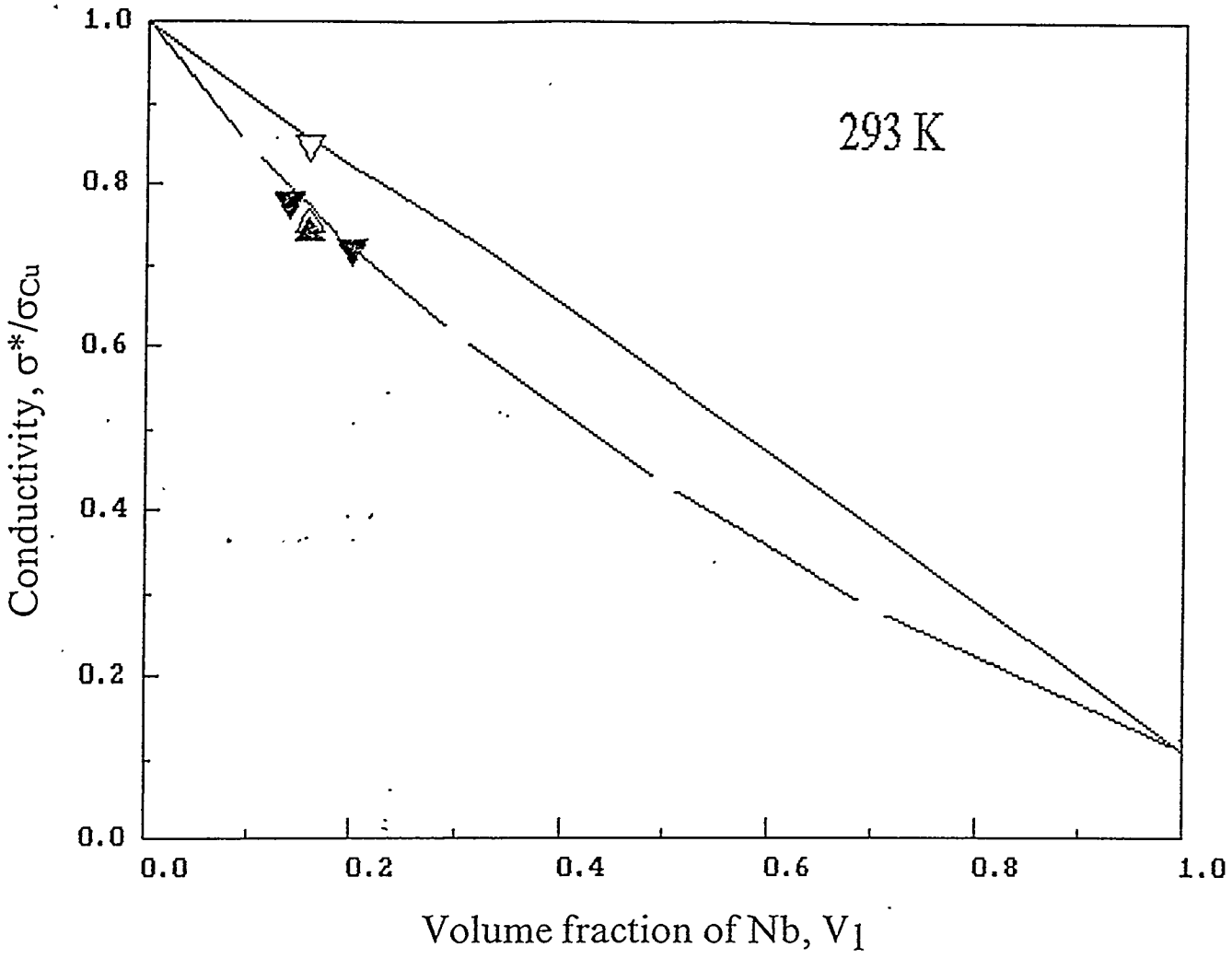

Fig. 17. Comparison of experimental values for conductivity of the Cu -Nb with calculations
——— - Equation (1); — — - Equation (2)
Δ - wire ∅0.8 (500°C - 1h), ▲ - wire ∅10 (500°C - 1h), ∇ - wire ∅3.0 (500°C - 1h), ▼ - rod 2 x 3

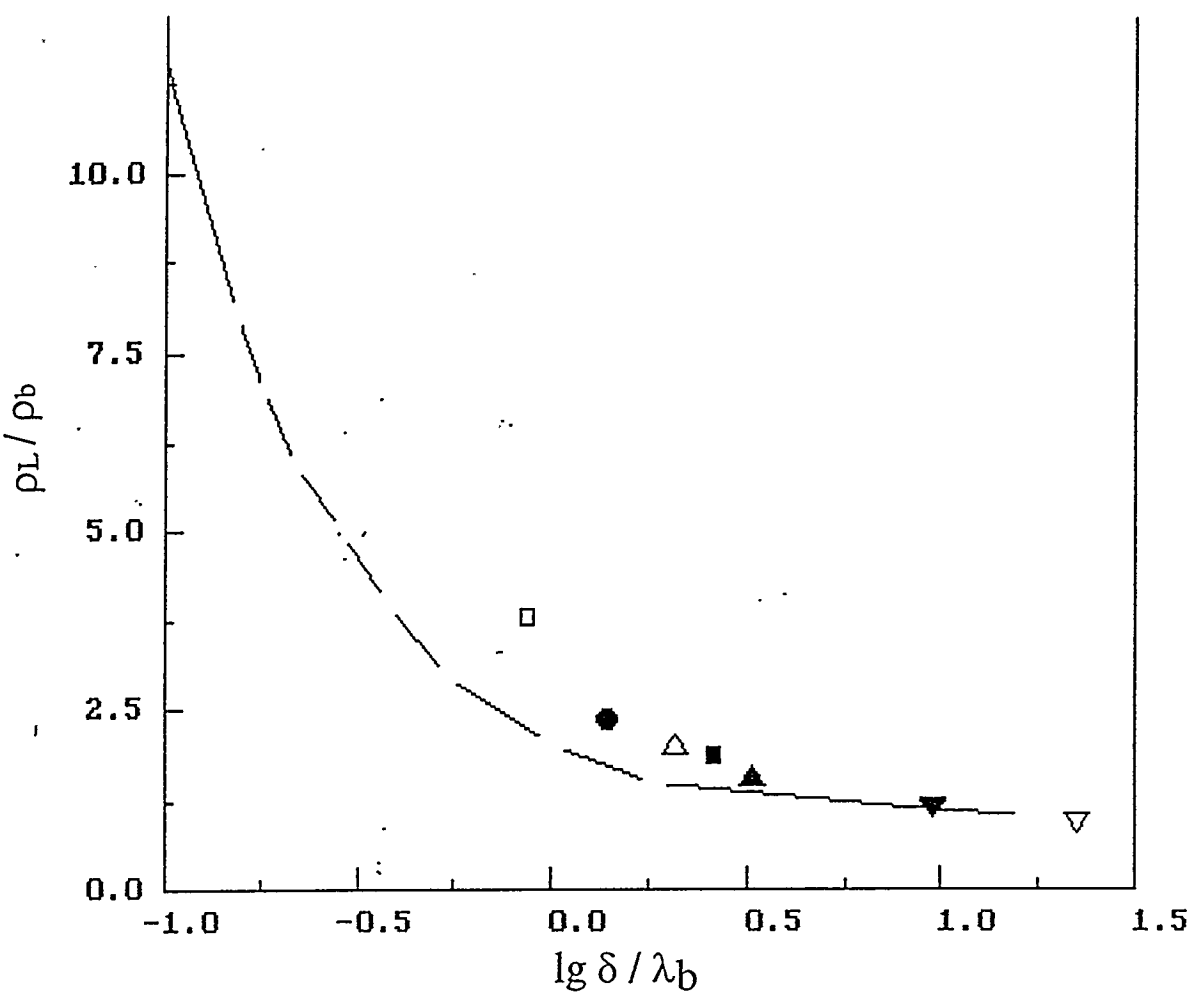

Fig. 18. The resistivity of copper (ρ_L) in Cu 16%Nb wire as a function of interfilament spacing (δ) .Comparison of experimental values with Sondheimer curve (- - - - -).
ρ_b, λ_b - resistivity and electron mean free path of the bulk copper.

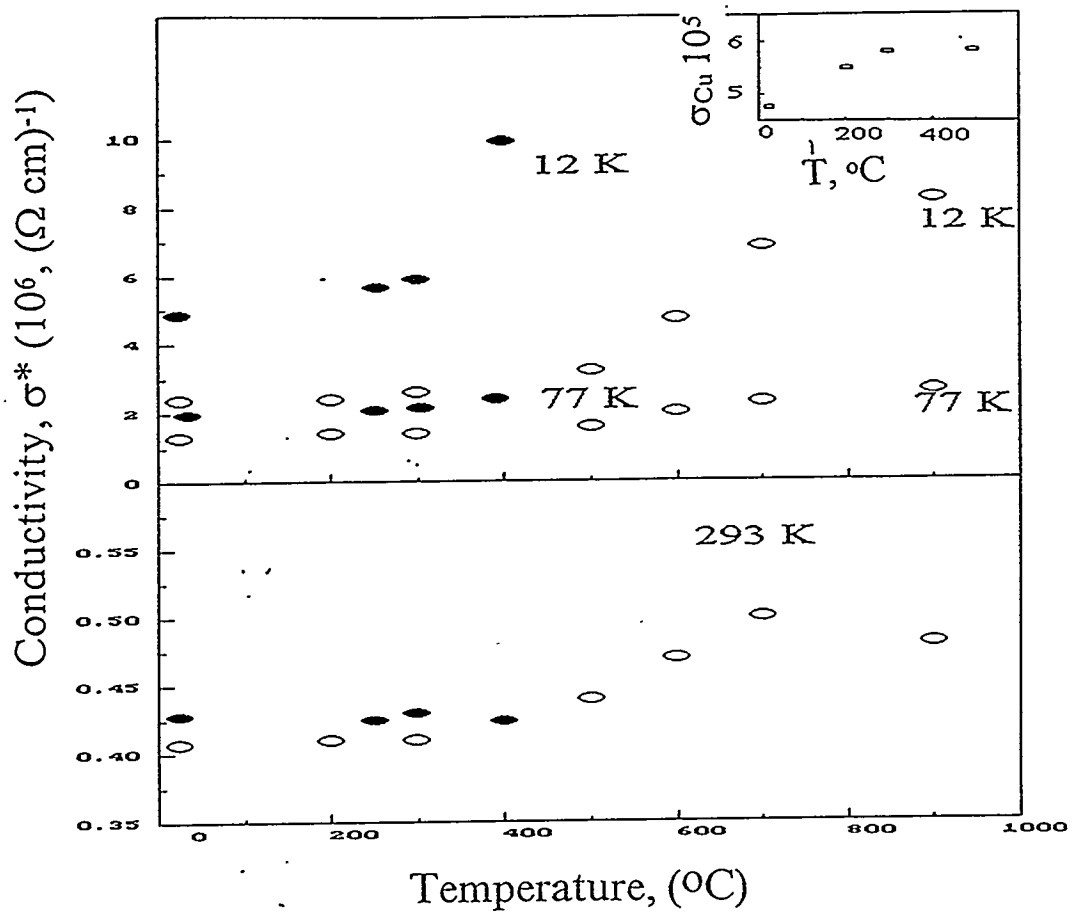

Fig. 19. Conductivity of Cu - 16%wtNb as a function of heat treatment temperature.
● - specimen № 6; o - specimen № 3. Inset - Conductivity of copper as a function of heat treatment.

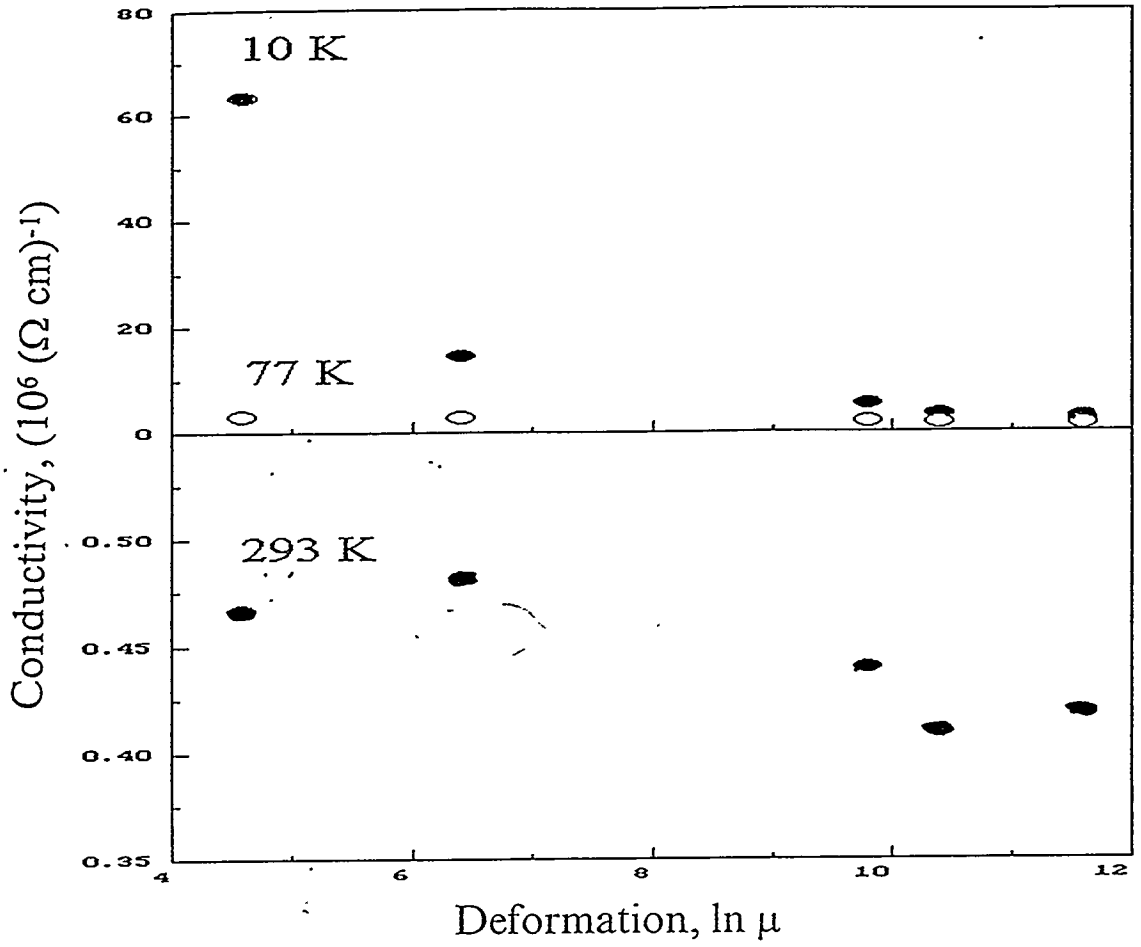

Fig. 20. Conductivity as a function of deformation.(Cu - 16wt%Nb) wire ∅ 0.8 mm heat treated at 500 °C for 1h.

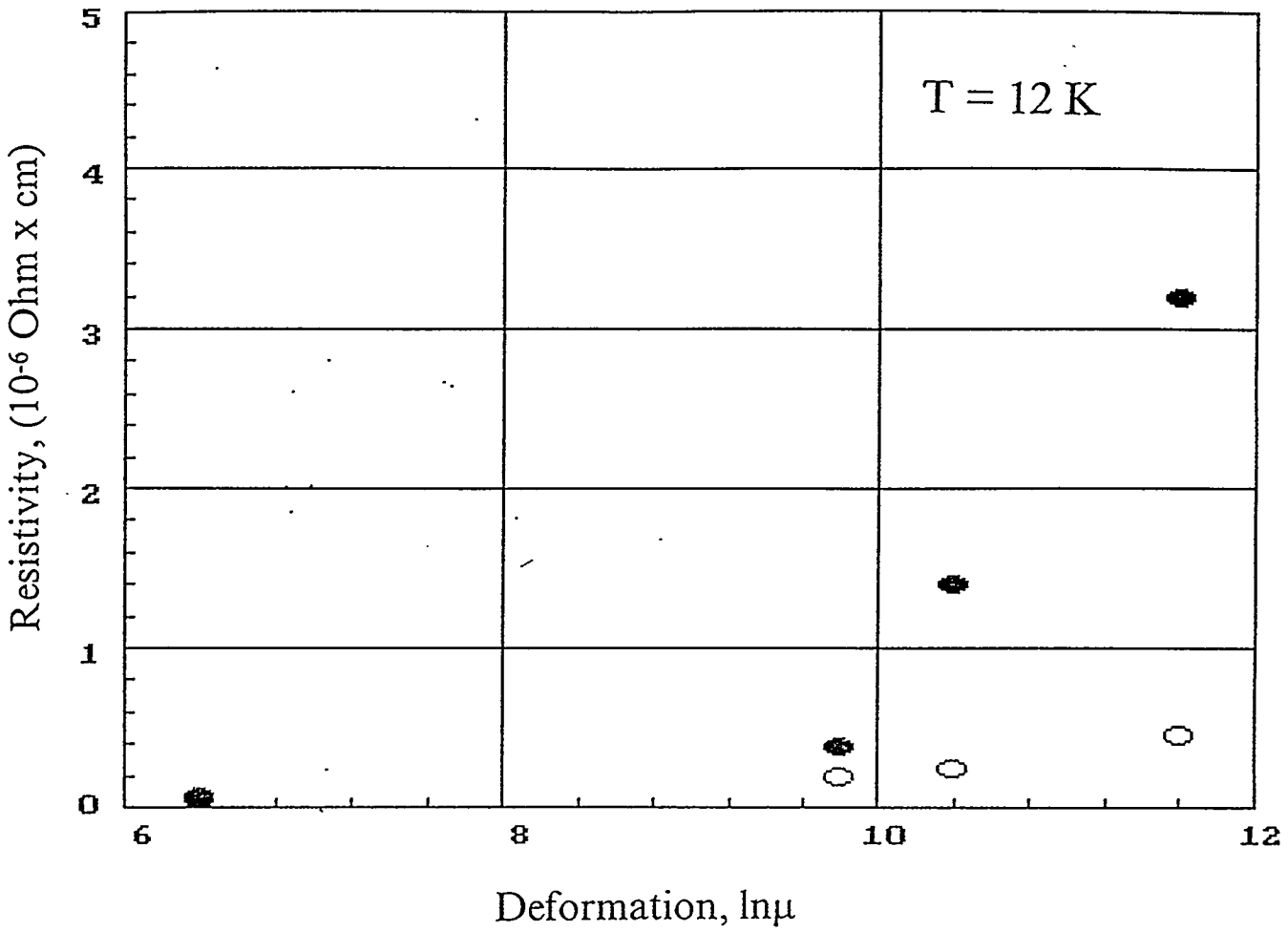

Fig. 21. Resistivity as a function of deformation
• - cold deformed; o - anneled at 500 ^{0}C, 1 h.

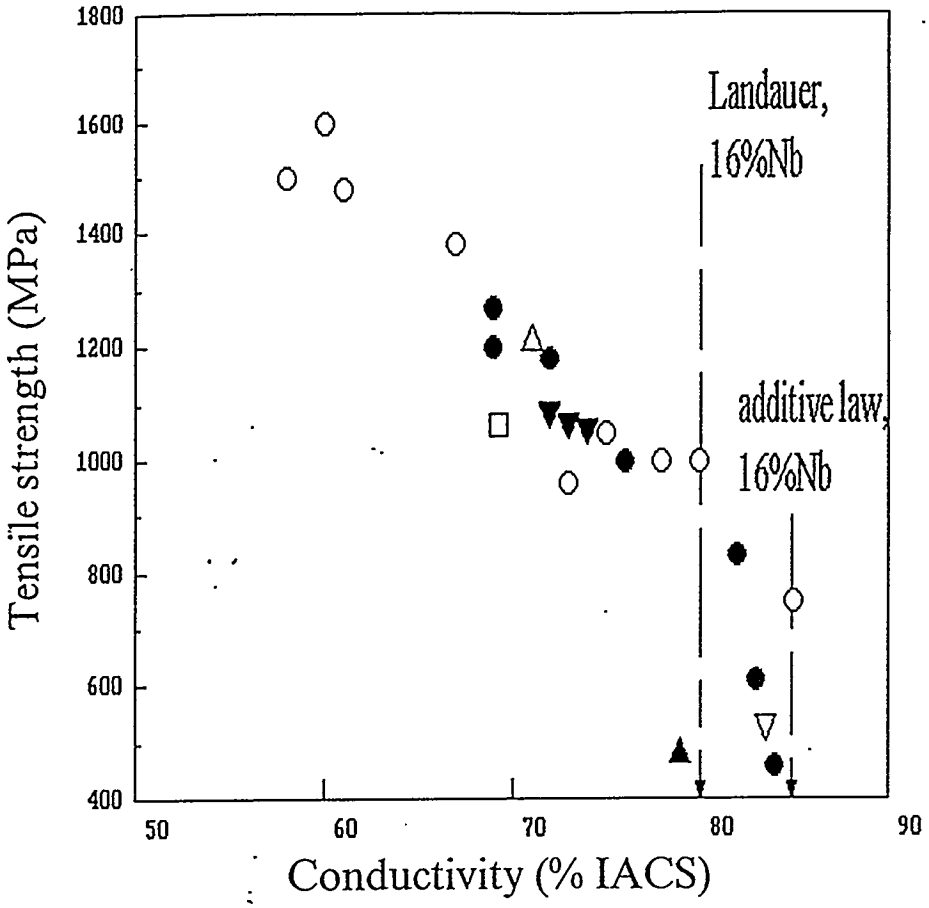

Fig. 22. Correlation between tensile strength and conductivity.
BARIIM wire (Cu - 16%Nb) with Cu matrix, ▾ - (2x3)mm,
O - ∅ 0.3mm;
wire (Cu - 16%Nb) without Cu matrix, ● - ∅ 0.8mm, ∇ - ∅ 3mm ▲- ∅ 10mm.
Supercon. (Cu - 22%Nb) - □. Ames (Cu - 15%Nb) - Δ.

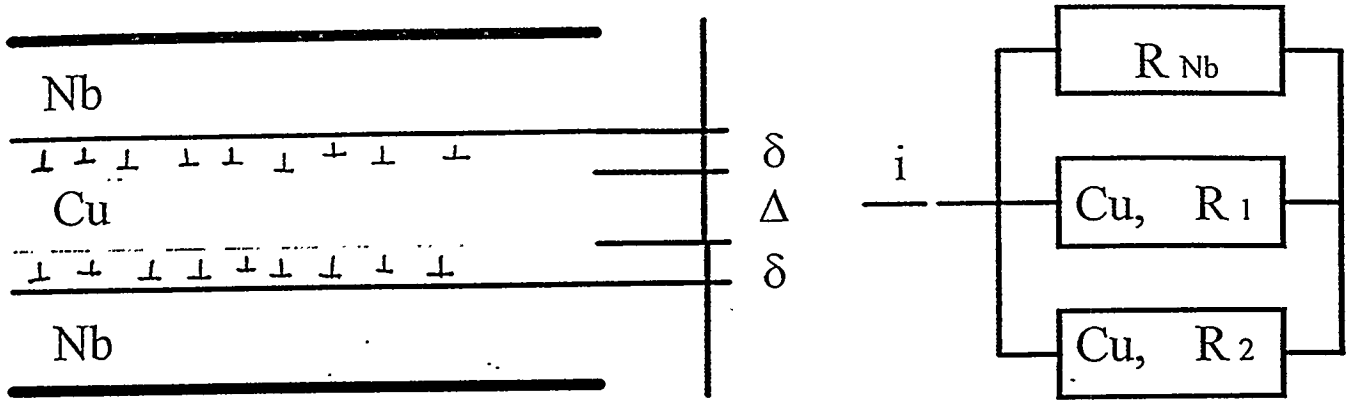

Fig. 23. Schematic of a structure of microcomposite and its electrical equivalent.

Fig 24

Superconductors for NMR-application

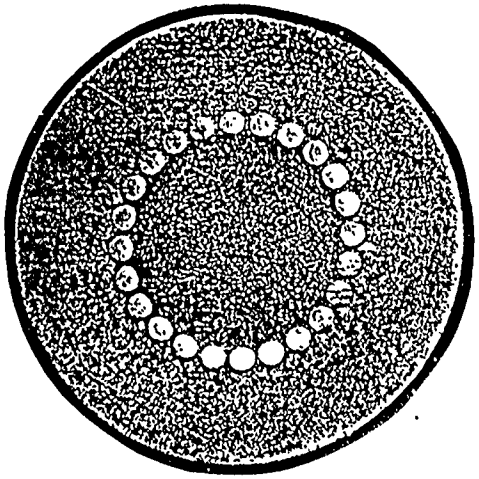

CKHT-0.08-24-1.45

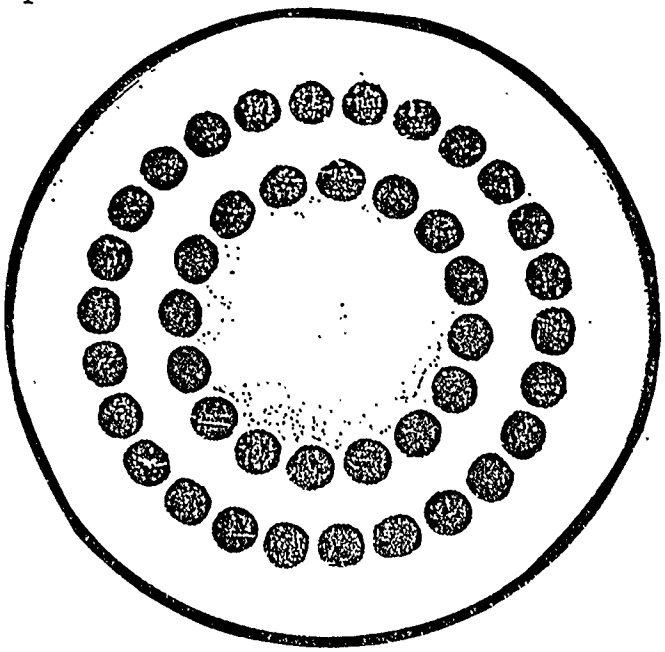

CKHT-0.25-42-0.82

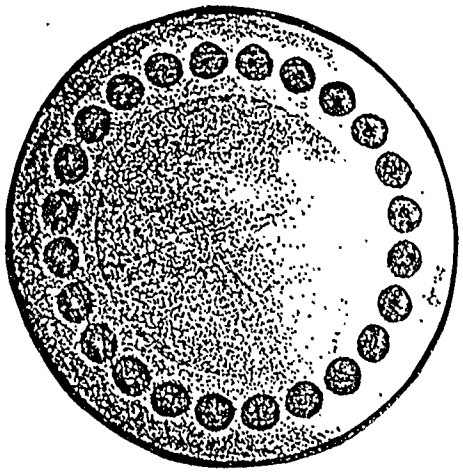

CKHT-0.12-24-0.85

	Wire diameter, mm	Number of filaments	Diameter of filament, mcm	Cu/NbTi	Critical current, A		
					1T	2T	3T
CKHT-0.25-42-0.82	0.82	42	62	3	-	700	535
CKNT-0.18-20-0.94	0.94	20	80	4.6	-	535	445
CKHT-0.16-18-0.85	0.85	18	70	5	560	-	260
CKNT-0.16-18-0.85*	0.85	18	70	5	640	420	310
CKHT-0.12-24-0.85	0.85	24	70	7	430	310	260
CKNT-0.12-24-1.25	1.25	24	88	7.5	-	655	540
CKHT-0.08-24-1.45	1.45	24	85	11	-	600	485
CKNT-0.08-24-1.75	1.75	24	103	11	855	735	690

* The wire has a resistent matrix